

NAVAL POSTGRADUATE SCHOOL

Monterey, California



THESIS

ALUMINUM 7075-T6 FATIGUE DATA GENERATION AND PROBABILISTIC LIFE PREDICTION FORMULATION

by

John G. Kemna

September 1998

Thesis Advisor:

Edward M. Wu

Approved for public release; distribution is unlimited.

DTIC QUALITY INSPECTED 3

19981201 117

REPORT DOCUMENTATION PAGE			Form Approved OMB No. 0704-0188	
Public reporting burden for this collection of information is estimated to average 1 hour per response, including the time for reviewing instruction, searching existing data sources, gathering and maintaining the data needed, and completing and reviewing the collection of information. Send comments regarding this burden estimate or any other aspect of this collection of information, including suggestions for reducing this burden, to Washington headquarters Services, Directorate for Information Operations and Reports, 1215 Jefferson Davis Highway, Suite 1204, Arlington, VA 22202-4302, and to the Office of Management and Budget, Paperwork Reduction Project (0704-0188) Washington DC 20503.				
1. AGENCY USE ONLY (Leave blank)		2. REPORT DATE September 1998		3. REPORT TYPE AND DATES COVERED Master's Thesis
4. TITLE AND SUBTITLE ALUMINUM 7075-T6 FATIGUE DATA GENERATION AND PROBABILISTIC LIFE PREDICTION FORMULATION			5. FUNDING NUMBERS Contract Number N0042198WR 14350	
6. AUTHOR(S) Kemna, John G.				
7. PERFORMING ORGANIZATION NAME(S) AND ADDRESS(ES) Naval Postgraduate School Monterey, CA 93943-5000			8. PERFORMING ORGANIZATION REPORT NUMBER	
9. SPONSORING / MONITORING AGENCY NAME(S) AND ADDRESS(ES) Commander, Naval Air Systems Command (PMA-290/SRP) Bldg. 2272, 47123 Buse Rd., Patuxent River, MD 20670			10. SPONSORING/MONITORING AGENCY REPORT NUMBER	
11. SUPPLEMENTARY NOTES The views expressed in this thesis are those of the author and do not reflect the official policy or position of the Department of Defense or the U.S. Government.				
12a. DISTRIBUTION / AVAILABILITY STATEMENT Approved for public release; distribution is unlimited.			12b. DISTRIBUTION CODE	
13. ABSTRACT (Maximum 200 words) The life extension of aging fleet aircraft requires an assessment of the safe-life remaining after refurbishment. Risk can be estimated by conventional deterministic fatigue analysis coupled with a subjective factor of safety. Alternatively, risk can be quantitatively and objectively predicted by probabilistic analysis. In this investigation, a general probabilistic life formulation is specialized for constant amplitude, fully reversed fatigue loading utilizing conventional breakdown laws applied to the general probability damage function. Experimental data was collected both as a bench mark data base, as well as an example of the implementation of probabilistic fatigue life prediction. Fully reversed, sinusoidal fatigue testing under load control was carried out at load levels giving high cycle fatigue lives from 1×10^4 to 5×10^6 cycles. The number of replications at each stress level is greater than currently available in the literature, thereby increasing the confidence of predictions in the long-life domain, as well as extending the statistical basis for probabilistic inference. The load level data sets are interpreted by the probabilistic damage function for life location as well as life shape parameters using maximum likelihood analysis. Homologous life ranking and the minimum entropy hypothesis are investigated as well.				
14. SUBJECT TERMS Aluminum 7075-T6, Fatigue Life Prediction, Fatigue Data Base, Probability, Reliability, Damage Accumulation, Maximum Likelihood Analysis			15. NUMBER OF PAGES 118	
			16. PRICE CODE	
17. SECURITY CLASSIFICATION OF REPORT Unclassified	18. SECURITY CLASSIFICATION OF THIS PAGE Unclassified	19. SECURITY CLASSIFICATION OF ABSTRACT Unclassified	20. LIMITATION OF ABSTRACT UL	

Approved for public release; distribution is unlimited

**ALUMINUM 7075-T6 FATIGUE DATA GENERATION AND PROBABILISTIC
LIFE PREDICTION FORMULATION**

John G. Kemna
Lieutenant, United States Navy
B.S., United States Naval Academy, 1989

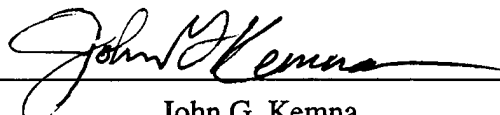
Submitted in partial fulfillment of the
requirements for the degree of

MASTER OF SCIENCE IN AERONAUTICAL ENGINEERING

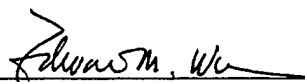
from the

**NAVAL POSTGRADUATE SCHOOL
September 1998**

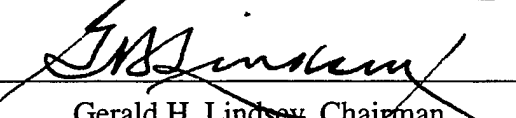
Author:


John G. Kemna

Approved by:


Edward M. Wu, Thesis Advisor


Gerald H. Lindsey, Second Reader


Gerald H. Lindsey, Chairman
Department of Aeronautics and Astronautics

ABSTRACT

The life extension of aging fleet aircraft requires an assessment of the safe-life remaining after refurbishment. Risk can be estimated by conventional deterministic fatigue analysis coupled with a subjective factor of safety. Alternatively, risk can be quantitatively and objectively predicted by probabilistic analysis. In this investigation, a general probabilistic life formulation is specialized for constant amplitude, fully reversed fatigue loading utilizing conventional breakdown laws applied to the general probability damage function. Experimental data was collected both as a bench mark data base, as well as an example of the implementation of probabilistic fatigue life prediction. Fully reversed, sinusoidal fatigue testing under load control was carried out at load levels giving high cycle fatigue lives from 1×10^4 to 5×10^6 cycles. The number of replications at each stress level is greater than currently available in the literature, thereby increasing the confidence of predictions in the long-life domain, as well as extending the statistical basis for probabilistic inference. The load level data sets are interpreted by the probabilistic damage function for life location as well as life shape parameters using maximum likelihood analysis. Homologous life ranking and the minimum entropy hypothesis are investigated as well.

TABLE OF CONTENTS

I.	INTRODUCTION.....	1
A.	BACKGROUND.....	1
B.	MOTIVATION	1
1.	Quantitative Risk Assessment or Life Extension.....	1
C.	SCOPE OF THIS THESIS	2
II.	PROBABILISTIC LIFE PREDICTION.....	5
A.	PROBABILISTIC MODEL.....	5
B.	FLAW DISTRIBUTION.....	6
C.	LIFE DISTRIBUTION.....	7
D.	HAZARD FUNCTION	7
III.	DAMAGE ACCUMULATION VIA LIFE CONVOLUTION	9
A.	FORMULATION.....	9
1.	Power Law Damage Function	9
2.	Exponential Form Damage Function	10
3.	Constant Stress Case Examples.....	10
4.	Alternating Stress Case Example	14
IV.	NPS ALUMINUM 7075-T6 FATIGUE DATA	17
A.	INTRODUCTION.....	17
1.	Data Set Descriptions	18
V.	DATA INTERPRETATION.....	19
A.	GENERALIZATION	19
B.	INITIAL INTERPRETATIONS	19
1.	Weakest Link Observations.....	19
C.	PARAMETER ESTIMATION OBSERVATIONS.....	21
D.	COMBINING THE DATA SETS.....	22
1.	Equivalent Stress Level Considerations.....	22
2.	Equivalent Life Considerations.....	25
E.	RESULTS OF COMBINED DATA SETS.....	29
F.	FINAL RESULTS.....	31
VI.	DAMAGE FUNCTION VISUALIZATION & DATA COMPARISON.....	35
1.	Traditional Methods	35
B.	COMPARISON TO EXPERIMENTAL PUBLISHED DATA.....	36
C.	DAMAGE FUNCTION FORM COMPARISONS TO EXPERIMENTAL DATA	37
VII.	FAILURE MECHANISMS	41

A.	FRACTURE MORPHOLOGY OBSERVATIONS	41
VIII.	CONSTANT AMPLITUDE FATIGUE TESTING.....	43
A.	INTRODUCTION.....	43
B.	TEST FACILITY & EQUIPMENT	43
1.	Load Frame.....	43
2.	Hydraulic Power Supply	44
3.	Servo Controller	45
C.	EXPERIMENTAL PROCEDURES	46
1.	Test Specimen Description.....	46
D.	CONSTANT AMPLITUDE FATIGUE TESTING PROCEDURES	47
1.	System Power Up	47
2.	Alignment.....	47
3.	Constant Amplitude System Tuning	48
4.	Coupon Testing Procedures.....	48
IX.	CONCLUSIONS & RECOMMENDATIONS	51
A.	CONCLUSIONS	51
B.	RECOMMENDATIONS	52
	LIST OF REFERENCES	55
	BIBLIOGRAPHY	57
	APPENDIX A. INITIAL DATA INTERPRETATION.....	59
	APPENDIX B. MLE PARAMETER SOLUTIONS.....	67
	APPENDIX C. NPS CONSTANT AMPLITUDE FATIGUE TEST PROCEDURES	95
	APPENDIX D. SPECIMEN DRAWINGS	101
	APPENDIX E. FAILED SPECIMEN PHOTOS	103
	INITIAL DISTRIBUTION LIST	107

ACKNOWLEDGEMENT

I must first thank my wife Stacia for her support, understanding and motivational inspiration throughout the long days, nights and months of this endeavor. I wish to thank my family for their continued support as well.

The author would like to acknowledge the financial support of the P-3C Class Desk Officer, Program Manager Air, Maritime Surveillance Aircraft (PMA-290) Sustained Readiness Program, for allowing the purchase of equipment, software, and support material used in this thesis. This work was performed under Contract N0042198WR14350. Also, I would like to thank Professor Lindsey for his guidance in the editing of this work.

Finally, I 'want' to thank my advisor, Professor (still throwing the "heat") Wu, for the opportunities provided in his pursuit of educating a "farm boy". His guidance, extraordinary dedication and perseverance were instrumental in the development of this thesis. I will forever be thankful for his inspirational thinking and work ethic throughout the rest of my career.

I. INTRODUCTION

A. BACKGROUND

As a result of tighter defense budgets and reductions in resources, the funding for replacement aircraft has diminished to the point that current fleet aircraft are under extensive life assessment and extension programs. The P-3 Orion, the Navy's Fleet Maritime Patrol Aircraft, has been under continuous service life assessment, extension and sustained readiness programs for many years now. The original service life of the aircraft has been extended such that the aircraft will need to be in service until well beyond the year 2000, which may include different flight profiles.

The overall objective is to quantitatively assess the reliability against failure for the remainder of the life of the aircraft. The most efficient method of obtaining this objective is through the use of a probabilistic life prediction model.

B. MOTIVATION

1. Quantitative Risk Assessment or Life Extension

The life extension of aging fleet aircraft requires an assessment of the safe-life remaining on non-refurbished components and structures as well as for those after refurbishment. Conventional deterministic fatigue analysis has allowed the community to use an *estimated* risk assessment. These risks can be estimated by applying a subjective factor of safety to a design life based on the mean of a small amount of data points taken at the stress levels and the amplitude ratios (R), in question. The design life is sometimes referred to as the median fatigue life as referred to in MIL-HDBK-5G [Ref. 1: p. 9-85]. The issue with this methodology is whether the variability of the fatigue life at the design loads or stress histories is adequately accounted for in the application of the factor of safety. This factor may be overly conservative in some cases, while less conservative in others.

Alternatively, risk can be quantitatively and objectively predicted by probabilistic analysis. Through this type of analysis, a more definitive risk assessment is fully realizable, leading to better decisions based on known variability in life with specific loading conditions and stress histories. Given this more definitive and formal approach, the result could save the Navy time, money, and aircraft as well as further enhance the safety of aircrew.

Constant amplitude stress histories (single level amplitude ratios, R) only require statistics to apply risk assessment analysis. However, for multiple load level, sequences and spectrum histories based on ground-air-ground (GAG) cycles, quantitative risk assessment requires a probabilistic damage function. Therefore, the main objective of this thesis is to provide a formulation and accumulate the probabilistic knowledge needed for this application.

C. SCOPE OF THIS THESIS

The purpose of this thesis was to build upon and continue the experimental and research efforts, which originated at NPS in 1996. In this investigation, a general probabilistic life formulation is specialized for constant amplitude, fully reversed fatigue loading. Experimental data was collected both as a bench mark data base as well as an example of the implementation of probabilistic fatigue life prediction. Fully reversed, sinusoidal fatigue testing under load control was carried out at load levels giving very high cycle fatigue lives from 10^4 to 5×10^7 cycles. The number of replications at each load level for these ranges is greater than can be found in the current literature, thereby extending the confidence of predictions into the long-life domain, as well as lending to the expansion of the statistical basis for probabilistic inference. Although the more general spectrum loading conditions can be predicted by the current formulation, they have not been experimentally carried out in this investigation.

In this investigation, specialized conventional breakdown laws (power law and exponential law) are applied to the general probabilistic damage function. The data sets collected at each level are interpreted by the probabilistic damage function for life location as well as life shape parameters using maximum likelihood analysis. Homologous life ranking (i.e., the strongest in terms of strength is equivalent to the

longest in terms of life) and a minimum entropy (least variability) hypothesis are also investigated. Future exploration is required in reconciling the strain control life prediction versus stress (load) controlled life prediction.

II. PROBABILISTIC LIFE PREDICTION

A. PROBABILISTIC MODEL

To effectively predict a single component's life, the probability density function, PDF or f , and the cumulative distribution function, CDF or F , of the component must be determined. This requires a sufficient amount of data, usually limited by time constraints and resources. However, to get an accurate statistical reliability estimate from direct testing, one must test a number of samples an order of magnitude greater than the desired reliability. In the case of military aircraft, the desired reliability is $0.99999 (1 - 10^{-5})$, which would require testing at least one million samples under this statistical approach. Therefore the analytical probabilistic approach based on experience and understanding of the physical phenomena is crucial in making reasonably accurate life predictions with the limited amount of data available.

Determination of the forms of the distributions requires breaking a component such as a spar web down into its constituent components whose distribution functions are known. This is similar to breaking down a spar web component into components the size of a normal fatigue testing coupon or specimen, which is the basis for this investigation.

The general probabilistic distribution for failure time was initiated by B. Coleman [Ref. 2], stating that the cumulative distribution function, CDF or F , of fatigue is a joint distribution of stress (S) and time (t) $\Rightarrow F(S, t)$. This was incorporated by Phoenix and Wu [Ref. 3, p.139] as follows:

$$F(t|S) = 1 - R(t|S) = 1 - \exp \left\{ - \Psi \left(\int_0^t \kappa(S(\xi)) d\xi \right) \right\}, t \geq 0 \quad (2.1)$$

where $S(t)$, $t \geq 0$ is the stress history, $\kappa(\cdot)$ is commonly referred to as the damage function or breakdown rule, and $\Psi(\cdot)$ is the shape function. The basis for this general formulation will be discussed in the following sections.

B. FLAW DISTRIBUTION

In order to properly formulate the general damage function, it is important to understand the basic underlying principles and physics behind the formulation. This begins with the distribution of flaws within the material itself. The intrinsic properties of a material, including the introduction of flaws and dislocations, are inherent to the material composition and the manufacturing process. In other words, there are flaws that deal with the nature of the material makeup and those that deal with the making of the material and the quality control that goes along with it.

The mechanistic basis for fatigue failure in metals is related to crack size and dislocation density. Failure of the material occurs when the flaws (crack size or dislocation density) increase and exceed a critical value. The test section of a fatigue specimen can be broken down into smaller constituent, yet equivalent metric volumes or crystals. The size of these volumes or crystals is arbitrary but bounded by the predetermined critical flaw size. If each crystal were microscopically inspected for flaws sizes greater than or equal to the critical size, the occurrence of flaws greater than or equal to critical value can be represented as p . Each crystal can be considered flawed (p) or not flawed (r). Thus there are only two possibilities for each crystal, pass or fail. Respective to the critical flaw size the exceedences are binomially distributed. Here again, p can be considered intrinsic to the manufacturing process or the quality control of the aluminum sheet used to make the fatigue test specimen.

According to Lewis [Ref. 4: p. 148], if the crystals are independent of one another and identically distributed, the reliability of the coupon can be written as:

$$R_n = P\{r_1 \cap r_2 \cap r_3 \cap \dots \cap r_n\} = P\{r_1\}P\{r_2\}P\{r_3\} \dots P\{r_n\}. \quad (2.2)$$

Equation 2.2 can be simply written as $R_n = r^n$ or $R_n = (1 - p)^n$. In the case of aircraft material components, the probability of occurrence of a flaw greater than the critical value within any metric volume must be very small. If the probability of a flaw, p , is very small then $\ln(1 - p) \cong -p$. Thus, the reliability of the coupon can then be represented as:

$$R_n = e^{-np}. \quad (2.3)$$

Therefore the binomial distribution has effectively been reduced to the Poisson distribution because the probability of a flaw is very small.

C. LIFE DISTRIBUTION

For any given instant in time, in order for a coupon to have life τ (fractional life consumed), each of the crystals, or metric volumes, must have life, τ which can be best characterized by the weakest link theory. In other words, when the weakest link or crystal fails, the chain or coupon fails. Again, the assumption is made that the reliability of each crystal is independent of the others and is identically distributed. The failure is also assumed to be homogeneous to mechanism or not related to the size of a coupon. A larger component will have more elements, but the flaw distribution does not change.

In exploring the weakest link theory further, the reliability of the coupon is:

$$R_n(p) = (1 - F_n(p)) = (1 - F(p))^n, \quad (2.4)$$

where $\ln(1 - F_n(p)) = n \ln(1 - F(p))$. Since $(1 - F_n(p))$ is always less than 1 because $F_n(p)$ is monotonically increasing, $\ln(1 - F_n(p))$ is always negative and the relation becomes:

$$\ln(-\ln(1 - F_n(p))) = \ln n + \ln(-\ln(1 - F(p))). \quad (2.5)$$

Equation (2.5) is most commonly referred to as the weakest link transformation for plotting realized data in the weakest link space. If the realized data were to plot as a straight line in this space, the distribution is said to follow that of the Weibull distribution. The Weibull distribution is generally written as:

$$F_{w_n}(p) = 1 - R_{w_n}(p) = 1 - e^{-n\left(\frac{p}{\beta}\right)^\alpha} = 1 - \left(e^{-\left(\frac{p}{\beta}\right)^\alpha}\right)^n. \quad (2.6)$$

D. HAZARD FUNCTION

The exponent in Equation (2.3), np , is referred to as the hazard, $\Psi(\tau)$, which relates to how the crystal deteriorates in general. In the fatigue process, the location parameter of the distribution of flaws is time dependent. As time increases, flaws grow and the probability that flaws exceed the critical size increases. Therefore, Equation (2.3) is just a snapshot in time and is generally represented as:

$$R_n(\tau) = e^{(-\Psi(\tau))}, \quad (2.7)$$

where τ is the fractional life consumed for the system. In the case in which the test sections of the coupons were smaller elements of a larger component, the reliability of the total population of test coupons could be written as:

$$R_N(\tau) = e^{(-\Psi(\tau))}. \quad (2.8)$$

In summary, the hazard function, $\Psi(\tau)$, is what describes the general nature of degradation induced by the fatigue process. The functional form of $\Psi(\tau)$ is very important because it describes the actual physical process in which flaws grow over time, $p(\tau)$.

Using the power form where $\Psi(\tau) = \tau^a$ seems to logically fit in most cases. This form is based on the power series expansion which gives is the reason for the exponent, a . The power term is a single term, non-integer because the stress (mechanism acting on the system and its components) is a stress norm or scalar. The derivative must always be greater than zero because $p(\tau)$ is always monotonically increasing. In other words, there is no self-healing process present. It is important to choose the form that best describes $p(\tau)$ (how it increases), which is what makes the fatigue process physically reasonable.

III. DAMAGE ACCUMULATION VIA LIFE CONVOLUTION

A. FORMULATION

The intrinsic normalized life or fractional life consumed, τ , for a given stress history, $S(t)$, is obtained by convoluting the effect of stress by means of a damage function (breakdown rule), κ .

$$\tau = \frac{1}{\hat{t}} \int_{t_i}^t \kappa(S(\xi)) d\xi. \quad (3.1)$$

\hat{t} is constant, has dimension of time, and serves to make τ non-dimensional due to the fact that Equation (2.1) (reliability or probability) has no dimension. $S(t)$ is a stress norm that is piecewise continuous in time t , t_i is the initial time and $\kappa(\cdot)$ is a damage function. $\kappa(\cdot)$ is the kernel or function that serves the purpose of properly modeling the cumulative damage effects over time, which in the simplest case reduces to the familiar Miner's rule, a linear superposition of damage.

Different failure mechanisms require different forms of the breakdown rule or combinations thereof. The two forms that will be investigated are the Power Law Damage function and the Exponential Law Damage Function.

1. Power Law Damage Function

The first proposed damage function is based on the power law. This form has been postulated to fit low cycle fatigue data in metals associated with yielding. The general form of the power law damage function is usually written as:

$$\kappa(S(\xi)) = \left(\frac{S(\xi)}{C_1} \right)^b, \quad (3.2)$$

where b is the non-integer power needed to prevent multiple terms. C_1 is the non-dimensionalizing intrinsic value of the material (the population capacity) where in most cases this is the true fracture strength of aluminum, σ_f . $\frac{S(\xi)}{C_1}$ is the fractional loading

better described as how close the stress history approaches the material limit (true fracture strength). Both b and C_1 are generally matched to the material constants.

2. Exponential Form Damage Function

The second proposed damage function is defined using an exponential form. This form has been postulated to fit high cycle fatigue data in metals associated with flaw growth.

$$\kappa(S(\xi)) = \frac{1}{C_2} \exp\left(\frac{S(\xi)}{C_3}\right). \quad (3.3)$$

$\frac{S(\xi)}{C_3}$ is again the fractional loading. C_3 is the intrinsic non-dimensionalizing constant.

C_2 is a non-dimensional constant related to the exponential of the stress intercept divided by the non-dimensionalizing value of C_3 . This equation has dimension of time, t .

3. Constant Stress Case Examples

Having developed the above forms of the damage functions, the solution approach for each form can be used to determine the parameters from a known stress history. Once the parameters are known, they can be used to predict $F(t | S)$ for another stress history.

For example, a constant stress case can be defined as shown in Equation (3.4):

$$S(t) = \begin{cases} 0 & t < t_0 \\ S & t > t_0 \end{cases} \quad (3.4)$$

a. Power Law Application

In applying this stress history to the power law form, the stress history simplifies to $S(\xi) = S$. The fractional life consumed becomes:

$$\tau = \frac{1}{\hat{t}} \int_{t_0}^t \left(\frac{S}{C_1}\right)^b d\xi = \frac{1}{\hat{t}} \left(\frac{S}{C_1}\right)^b \int_{t_0}^t d\xi = \frac{t - t_0}{\hat{t}} \left(\frac{S}{C_1}\right)^b. \quad (3.5)$$

Substituting Equation (3.5) into the hazard equation, $\psi(\tau) = \tau^a$, gives:

$$\psi(\tau) = \left(\left(\frac{S}{C_1} \right)^b \frac{t - t_0}{\hat{t}} \right)^a. \quad (3.6)$$

Substituting Equation (3.6) into the Reliability equation, Equation (2.8), yields:

$$R(t) = \exp \left\{ - \left(\left(\frac{S}{C_1} \right)^b \frac{t - t_0}{\hat{t}} \right)^a \right\}. \quad (3.7)$$

If the data were to be consistent with that of a Weibull distribution, then Equation (3.7) can be compared to the Weibull form to match the parameters (i.e., $R(t) = R_w(t)$). For instance:

$$\exp \left\{ - \left(\left(\frac{S}{C_1} \right)^b \frac{t - t_0}{\hat{t}} \right)^a \right\} = \exp \left\{ - \frac{t}{t_\beta} \right\}^\alpha, \quad (3.8)$$

where α is the shape parameter and t_β is the location parameter. Equation (3.8) can be simplified to:

$$\left(\left(\frac{S}{C_1} \right)^b \frac{t - t_0}{\hat{t}} \right)^a = \left(\frac{t}{t_\beta} \right)^\alpha. \quad (3.9)$$

If $t_0 = 0$, and the shape parameter is related to the exponent a ($\alpha = a$), Equation (3.9) reduces to:

$$\left(\frac{S}{C_1} \right)^b \frac{t_\beta}{\hat{t}} = 1. \quad (3.10)$$

Expansion of Equation (3.10) into the logarithmic form yields:

$$b \log_e(S) + \log_e \left(\frac{t_\beta}{\hat{t}} \right) = b \log_e(C_1). \quad (3.11)$$

Equation (3.11) is thus linear in a $\log(S) - \log(t_\beta)$ domain where the slope is $-\frac{1}{b}$ with an intercept of $\log_e(C_1)$ as shown in Figure 3.1.

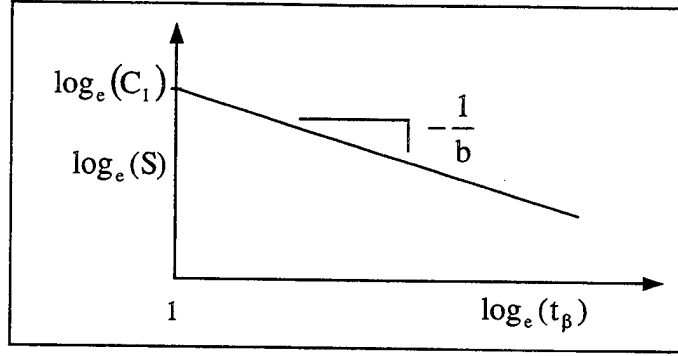


Figure 3.1. Constant Stress Power Relation

The comparison to the Weibull form allows the use of the Weibull parameters to formulate the damage function once the data has been proven to fit a Weibull distribution.

b. Exponential Law Application

Utilization of the same methodology as described for the power law example, the exponential law form can also be pursued. Again, in the case of a constant stress history as described above, $S(\xi) = S$. The stress tensor is a stress norm or scalar. The fractional life consumed thus becomes:

$$\tau = \frac{1}{\hat{t}} \int_{t_0}^t \frac{1}{C_2} \exp\left(\frac{S(\xi)}{C_3}\right) d\xi = \frac{1}{C_2} \exp\left(\frac{S}{C_3}\right) \frac{(t - t_0)}{\hat{t}}. \quad (3.12)$$

Here again, if $t_0 = 0$, then Equation (3.12) simplifies to:

$$\tau = \left(\frac{1}{C_2} \exp\left(\frac{S}{C_3}\right) \right) \frac{t}{\hat{t}}. \quad (3.13)$$

Substitution of Equation (3.13) into the hazard function yields:

$$\psi(\tau) = \left(\left(\frac{1}{C_2} \exp\left(\frac{S}{C_3}\right) \right) \frac{t}{\hat{t}} \right)^a. \quad (3.14)$$

Substitution of Equation (3.14) into Equation (2.1), thus reveals:

$$R(t) = \exp \left\{ - \left(\left(\frac{1}{C_2} \exp\left(\frac{S}{C_3}\right) \right) \frac{t}{\hat{t}} \right)^a \right\}. \quad (3.15)$$

Again, if the data were to be consistent with that of a Weibull distribution, Equation (3.15) can be compared to the Weibull form as such:

$$\exp\left\{-\left(\left(\frac{1}{C_2} \exp\left(\frac{S}{C_3}\right)\right)\frac{t}{\hat{t}}\right)^a\right\} = \exp\left\{-\frac{t}{t_\beta}\right\}^\alpha. \quad (3.16)$$

Equation (3.16) can then be simplified to:

$$\left(\frac{t}{t_\beta}\right)^\alpha = \left(\frac{1}{C_2} \exp\left(\frac{S}{C_3}\right)\right)\frac{t}{\hat{t}}. \quad (3.17)$$

The Weibull shape parameter, α , can again be related to the exponent a , where $\alpha = a$.

The relation then becomes:

$$\frac{t}{t_\beta} = \frac{1}{C_2} \exp\left(\frac{S}{C_3}\right)\frac{t}{\hat{t}}. \quad (3.18)$$

Further simplification and rearranging terms in Equation (3.18) yields:

$$C_2 = \frac{t_\beta}{\hat{t}} \exp\left(\frac{S}{C_3}\right). \quad (3.19)$$

Expansion of Equation (3.19) into the logarithmic domain yields:

$$\log_e\left(\exp\left(-\frac{S}{C_3}\right)\right) = \log_e\left(\frac{t_\beta}{\hat{t}}\right) + \log_e\left(\frac{1}{C_2}\right). \quad (3.20)$$

Simplification of Equation (3.20) gives a more familiar form:

$$S = -C_3 \log_e\left(\frac{t_\beta}{\hat{t}}\right) + \log_e(C_2). \quad (3.21)$$

Equation (3.21) is thus linear in a stress-log t_β semi-Log space and is illustrated in Figure 3.2. The slope is $-C_3$ and the intercept is C_2 or:

$$C_2 = \exp\left(\frac{S}{C_3}\right). \quad (3.22)$$

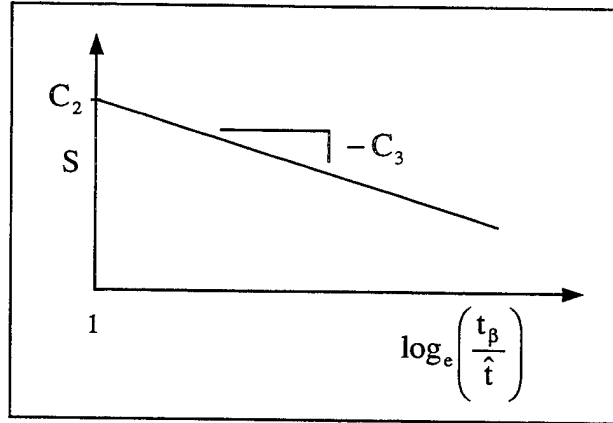


Figure 3.2. Constant Stress Exponential Relation

Therefore, if the Weibull parameters of the needed stress histories are found through experimental data, the generalized form of the damage function can then be determined.

4. Alternating Stress Case Example

Fatigue testing for this investigation was done using stress control with a fully reversed sinusoidal wave form which can be modeled as:

$$S(t) = \int_{t_i}^{t_f} S_a \sin\left(\frac{2\pi}{t_p} \xi\right) d\xi. \quad (3.23)$$

t_p is the period, S_a is the stress norm amplitude and $S(t)$ is the stress norm history with time. In the case of using the power law damage function the fractional life consumed, τ , over time, t then becomes:

$$\tau = \frac{1}{t} \int_{t_i}^{t_f} \left[\frac{S_a}{C_1} \sin\left(\frac{2\pi}{t_p} \xi\right) \right]^b d\xi. \quad (3.24)$$

The damage function for this case is therefore:

$$\kappa(S_a(\xi)) = \left(\frac{S_a}{C_1} \sin\left(\frac{2\pi}{t_p} \xi\right) \right)^b. \quad (3.25)$$

Unlike the previous constant stress cases, the integrand in Equation (3.24) is not symbolically integrable. Therefore, the integral must either be solved numerically or approximated. However, in the same case examples, the integration is the area under the curve of the stress history. This methodology may be applied to the constant amplitude

case in that the area under the curve over time will be a constant. The constant amplitude, sinusoidal stress case can then be reduced to an equivalent constant stress and can be related to the same forms of the damage functions formulated in constant stress case examples. For instance, Equation (3.25) can be represented in the same manner as Equation (3.2). Therefore, the constant amplitude stress history damage function can then be related in the same manner as was done in the constant stress history solutions with the resultant damage function differing only by a constant.

IV. NPS ALUMINUM 7075-T6 FATIGUE DATA

A. INTRODUCTION

Fully reversed sinusoidal fatigue tests under load (stress) control were carried out at load levels giving high cycle fatigue lives (10^4 to 5×10^6 cycles) As previously stated, the number of replications is greater than available in literature. NPS constant amplitude, load controlled fatigue testing was originated during thesis work conducted by LT Todd Kousky in 1996 [Ref. 5:p. 47]. This testing was done at medium and low stress levels of 30.9 and 25.6 kilo-pounds per square inch (ksi), respectively. For this investigation, tests were conducted at the lower stress level of 25.6 ksi and then further extended to a higher stress level of 51.2 ksi. In all, 119 coupon specimens were tested until failure with 36 conducted at the high stress level, 23 at the medium stress level and 39 at the low stress level.

Throughout the course of this thesis research, testing equipment and techniques were further refined to increase the level of confidence in the data being collected. The overall breakdown of the number of tests completed at each of the test conditions and stress levels have been depicted in a data matrix, $\{D_{ij}\}$, as shown in Table 4.1. A

Stress Level	Servo Control Device / Accessory / Technique			
	Analog	Analog ₍₁₎	Digital ₍₁₎	Digital _(1,2)
High				36
Medium	23			
Low	7	9	8	15

Notes: (1) refined gripping technique, (2) amplitude control

Table 4.1. Data Set Matrix, $\{D_{ij}\}$

description of each note can be found in Chapter VIII.

1. Data Set Descriptions

The rows of the data matrix, ($i = 1, 2, 3$), pertain to the high, medium and low stress levels of testing conducted at 51.2, 30.9, and 25.6 ksi, respectively. The columns, ($j = 1, 2, 3, 4$) denote the different methods and equipment used in the collection of each data set. A description of each of the features and techniques can be found in Chapter VIII.

Data sets, $\{D_{i1}\}$ were collected using an older analog controller (circa 1975 technology), which was the only servo control device available for use at the time. Data set $\{D_{i2}\}$ was collected with the same controller but a more refined gripping technique was instituted due to problems encountered with specimens breaking in the gripping sections. This technique was subsequently applied to the remaining data sets.

Through funding provided by the research sponsor, a modern digital controller was purchased and used to collect data sets $\{D_{i3}\}$ and $\{D_{i4}\}$. This new digital controller (circa 1997) provided more capability in control and tuning, which further enhanced confidence in the data being collected. Data sets $\{D_{i4}\}$ were produced with the highest experimental technique refinement which included the previously mentioned amplitude control feature. This feature eliminated small drifts in amplitude that had to be closely observed and manually adjusted in the previous data set, $\{D_{i3}\}$. Data collected in data sets $\{D_{i4}\}$ are the main emphasis of this investigation.

V. DATA INTERPRETATION

A. GENERALIZATION

Engineering fatigue data collection is typically done either under strain control for low cycle fatigue or load (stress) control for high cycle fatigue. The actual structures themselves experience mixed strain and stress conditions. In order to further formulate the general probabilistic damage function, the data sets collected under the different methods and load levels needed to be interpreted using probabilistic methodologies such as parameter estimation for life location as well as life variability.

B. INITIAL INTERPRETATIONS

1. Weakest Link Observations

The first step in interpreting the data consisted of plotting each of the data sets in the weakest link space as discussed in Chapter II. The exact realized random variables, x_{n_i} , of each data set $\{D_{ij}\}$, were compiled in the order of testing sequence. The data was then sorted and ranked in order of life or cycles to failure (i.e., weakest to the strongest specimen). The expected rank, \tilde{F} , was calculated as:

$$\tilde{F} = \frac{n}{N+1}, \quad (5.1)$$

where n is the rank in order of life and N is the total number of realized data in the data set $\{D_{ij}\}$. The weakest link transformation was performed as shown in Equation (5.2).

$$F^* = \ln(-\ln(1 - \tilde{F})). \quad (5.2)$$

The realized data was then plotted in the weakest link space, F^* vs. x_{n_i} , for each data set. As an example, the data set $\{D_{14}\}$, is shown in Table 5.1.

Specimen No.	Cycles(N_f)	Specimen No.	Cycles(N_f)	Specimen No.	Cycles(N_f)
1	8617	13	12421	25	12206
2	11283	14	10748	26	11272
3	10699	15	10120	27	11630
4	11200	16	13550	28	11785
5	7804	17	11972	29	12121
6	10481	18	9825	30	9502
7	8503	19	12996	31	11090
8	8263	20	10833	32	9809
9	11309	21	10457	33	10988
10	7574	22	10333	34	9769
11	10154	23	11109	35	9492
12	11906	24	10461	36	10466

Table 5.1. $\{D_{14}\}$, High Stress Level "Exact" Data

The weakest link plot for this data set is shown in Figure 5.1.

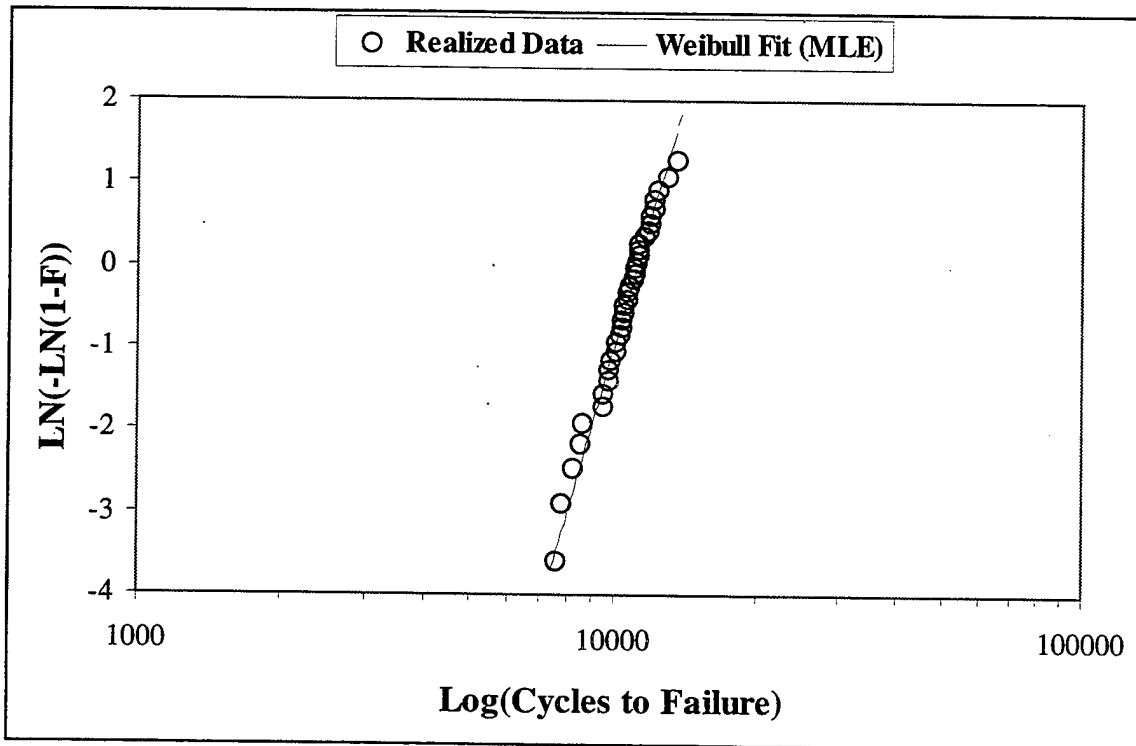


Figure 5.1. $\{D_{14}\}$ Weakest Link Plot

Figure 5.1 shows the data in $\{D_{14}\}$ very nearly plots as a straight line in the weakest link space. Therefore, it can be safely assumed this data can be represented by a

Weibull distribution. Appendix A contains the Data Tables and Weakest Link Plots of all data sets. Each of the data sets consistently followed the same approximate straight line trend in the weakest link space. With these observations, further analysis of the data was then pursued to determine the Weibull distribution shape (α) and location (β) parameters.

C. PARAMETER ESTIMATION OBSERVATIONS

One rudimentary method of parameter estimation is by a least squares fit of linearized data. However, least squares provides an equal weighting of the data which does not account for data cluster. A better and more sophisticated method called the Maximum Likelihood Estimate (MLE) weights the data by probability.

For each exact data set $\{D_{ij}\}$ with Weibull pdf, $f_w(x_n; \alpha_{ij}, \beta_{ij})$, the joint density function for the observation can be written as the *likelihood* function, $L_{ij}(x_n; \alpha_{ij}, \beta_{ij})$:

$$L_{ij}(D_{ij} | f_w(x_n; \alpha_{ij}, \beta_{ij})) = f_w(x_1; \alpha_{ij}, \beta_{ij}) f_w(x_2; \alpha_{ij}, \beta_{ij}) \dots f_w(x_n; \alpha_{ij}, \beta_{ij}). \quad (5.3)$$

The *maximum likelihood* can be obtained by taking the derivative of $L(\cdot)$ with respect to the parameters and setting it equal to zero. In this case, where the likelihood is based on two parameters, the software package uses an iterative method to obtain the simultaneous solution where $\frac{\partial L}{\partial \alpha} = 0$ and $\frac{\partial L}{\partial \beta} = 0$. Hence, maximum likelihood parameter estimation,

MLE, determines the values of α_{ij} and β_{ij} that provide the highest likelihood of observing the given set of data, $\{D_{ij}\}$.

At NPS, Professor Edward M. Wu has developed an MLE software package for this research that handles exact, censored and interval data. This software consisted of a program written in MATLAB by Professor Wu and was utilized to determine the parameters for each of the data sets. The solution of the maximum likelihood estimations for the data sets can be found in Appendix B. The results have been tabulated in Table 5.2.

$\{D_{ij}\}$	$\{D_{i1}\}$	$\{D_{i2}\}$	$\{D_{i3}\}$	$\{D_{i4}\}$
$\{D_{1j}\}$				$\alpha_{14} = 8.9$ $\beta_{14} = 1.12 \times 10^4$
$\{D_{2j}\}$	$\alpha_{21} = 3.1$ $\beta_{21} = 6.92 \times 10^4$			
$\{D_{3j}\}$	$\alpha_{31} = 1.5$ $\beta_{31} = 2.42 \times 10^5$	$\alpha_{32} = 1.2$ $\beta_{32} = 1.61 \times 10^6$	$\alpha_{33} = 7.5$ $\beta_{33} = 3.22 \times 10^6$	$\alpha_{34} = 4.2$ $\beta_{34} = 3.29 \times 10^6$

Table 5.2. Weibull Parameters, Initial Data Sets

These preliminary observations clearly show the differences between the two different controllers and the personnel conducting the tests. This emphasizes the need for continuity of personnel conducting the tests and the equipment being used.

D. COMBINING THE DATA SETS

In order to better utilize the data collected, regardless of method, further interpretation and analysis was needed to determine which data sets could be combined. Combining the data sets provided more observations to obtain more substantial results with the limited number of data collected. The goal was to merge the data sets into one single column in the data set table using proper methodologies such as data censoring and equivalent life (rank is homologous) maximum likelihood analysis.

1. Equivalent Stress Level Considerations

There were four different sets of data observed at the low stress level, $\{D_{3j}\}$. Each data set contained only a few data points with $\{D_{34}\}$ containing 15 exact data points. The data observed in $\{D_{34}\}$ was collected with the most refined testing equipment (digital controller with amplitude control) and therefore the remainder of the data sets at the low stress level were considered for merging into this data set.

a. *Combining $\{D_{34}\}$ and $\{D_{33}\}$*

The first set considered for merging into $\{D_{34}\}$ was $\{D_{33}\}$ since the data in this set did not exhibit more disorder than in $\{D_{34}\}$ (i.e., $\alpha_{33} > \alpha_{34}$). The location parameters were also essentially the same with $\beta_{33} \cong \beta_{34}$. Therefore it was judged appropriate to combine these two data sets into one represented as:

$$\{D_3\}_e = \{D_{33}\} \cup \{D_{34}\}, \quad (5.4)$$

where the subscript e denotes the data set is exact data. The data set was then analyzed using the MLE software where $\text{MLE } \alpha, \beta | \{D_{33}, D_{34}\}$ yielded $\alpha_{3_e} = 4.8$ and $\beta_{3_e} = 3.276 \times 10^6$. The merged data set (darkened circles) is plotted in the weakest

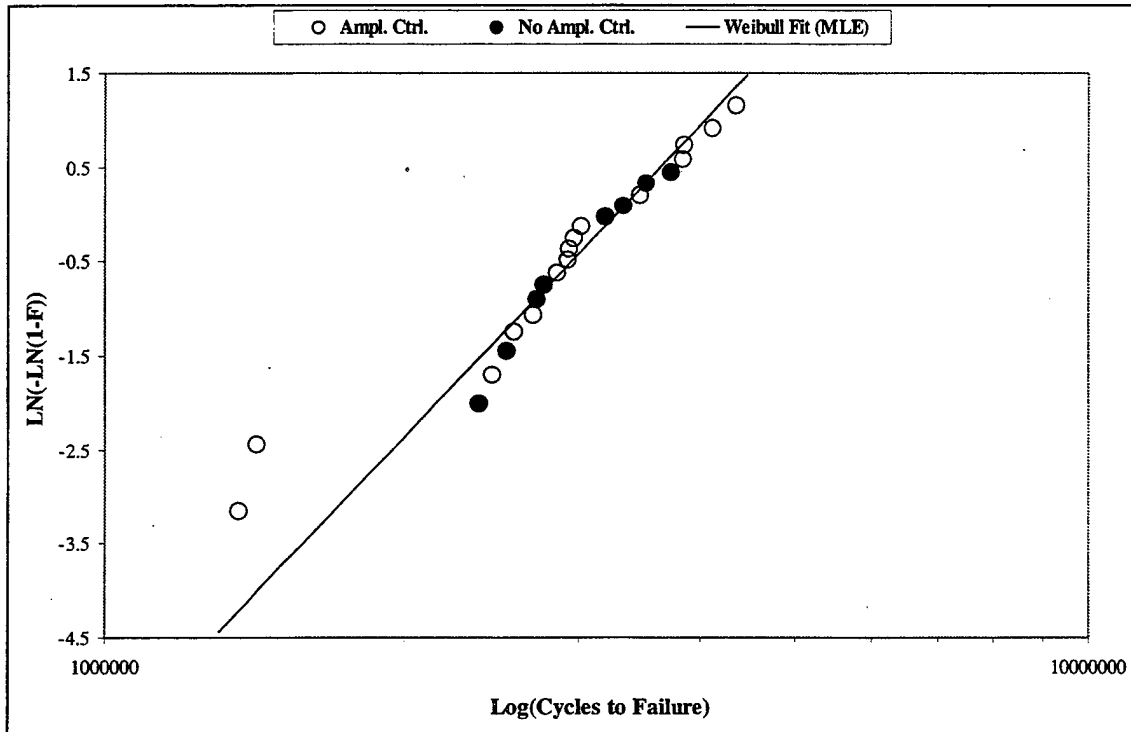


Figure 5.2. $\{D_3\}_e$ Weakest Link Plot, Merged Data

link space as shown in Figure 5.2. The MLE software output with the parameter solutions can be found in Appendix B.

b. Data Sets $\{D_{31}\}$ and $\{D_{32}\}$

These data sets exhibited shape parameters much less than those corresponding to $\{D_{33}\}$ and $\{D_{34}\}$. The location parameter values were also much less. This could be based on two separate issues: (1) the failure mechanism is different than that of testing at the same stress level, and (2) the different testing conditions and equipment may have caused the added variance and lesser value of life location. This second issue could have involved higher than desired stress levels as a result of controller inaccuracies, hence, the shorter lives.

It was further observed that the shorter life data sets would have had to exhibit a different failure mechanism than the longer life data sets at the same stress level. Therefore, it was judged more appropriate to attribute this difference to the different testing conditions and therefore it would only be appropriate to merge the data from these sets into $\{D_3\}_e$ by means of proper censoring techniques. To be specific, the data in sets $\{D_{31}\}$ and $\{D_{32}\}$ were considered as right censored data since the life of each specimen under these test conditions observed to be less than expected. This may have been due to possibly higher stress amplitude conditions under lesser refined test procedures. The censored data set for these two data sets then becomes $\{D_3\}_r = \{D_{31}\}_r \cup \{D_{32}\}_r$, where the subscript r denotes the right censoring of the data. The resultant data set from combining the censored data with the data set $\{D_3\}_e$ becomes:

$$\{D_3\}_{e,r} = \{D_3\}_e \cup \{D_{31}\}_r \cup \{D_{32}\}_r. \quad (5.5)$$

The subsequent MLE solution, written as $\text{MLE} \alpha, \beta | \{D_{33}, D_{34}, D_{31r}, D_{32r}\}$, yielded $\alpha_{3e,r} = 5.0$ and $\beta_{3e,r} = 3.333 \times 10^6$. The weakest link plot for this merged data set is shown in Figure 5.3 with the parameter solutions in Appendix B.

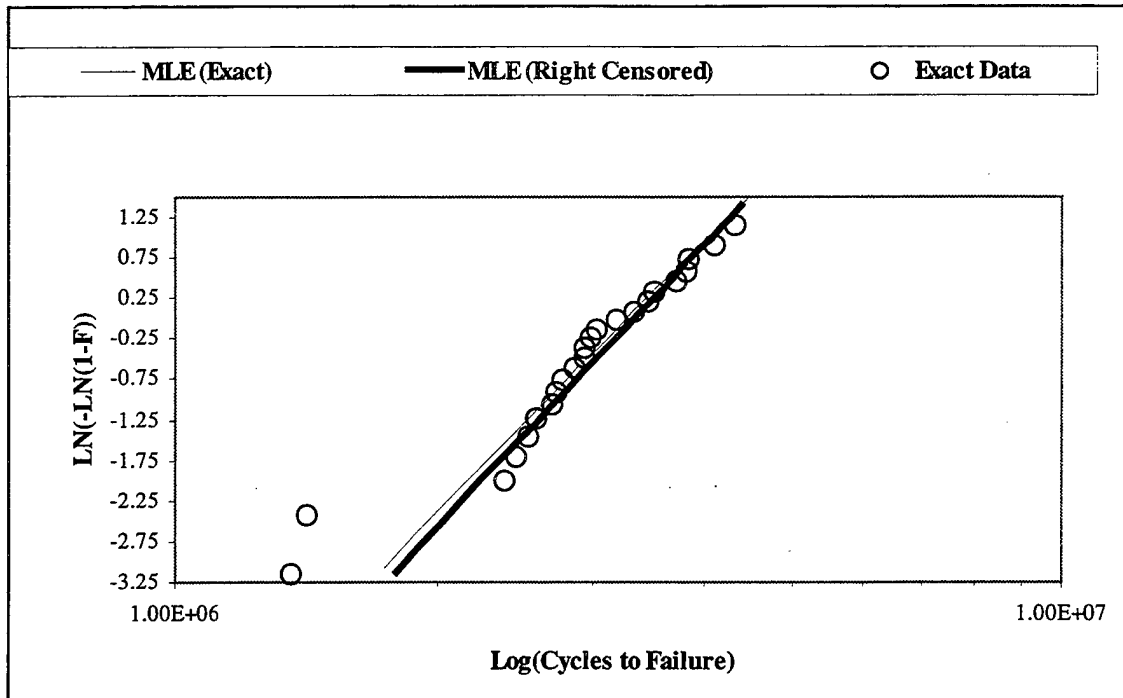


Figure 5.3. $\{D_3\}_{e,r}$ Weakest Link Plot, "Exact" Data

The resulting shape parameter increased slightly from 4.8 to 5.0 when comparing the censored data to the exact data parameter estimation. The same slight increase is also observed in the location parameter. The reason for this unexpected increase may be due to four points in data set $\{D_{32}\}$ that were somewhat close to the location parameter of the exact data set. These data however, must still be considered part of the censored data set because they were tested under the same conditions as the remainder of the data in the set.

2. Equivalent Life Considerations

a. Introduction

The concept of equivalent life where rank is homologous was also applied in the scope of this thesis to project the data collected at a higher stress level to the data set collected at a lower stress level. Figure 5.5 illustrates the projection using a slope, ρ_1 , where the slope is unknown because the damage function between the stress levels is unknown.

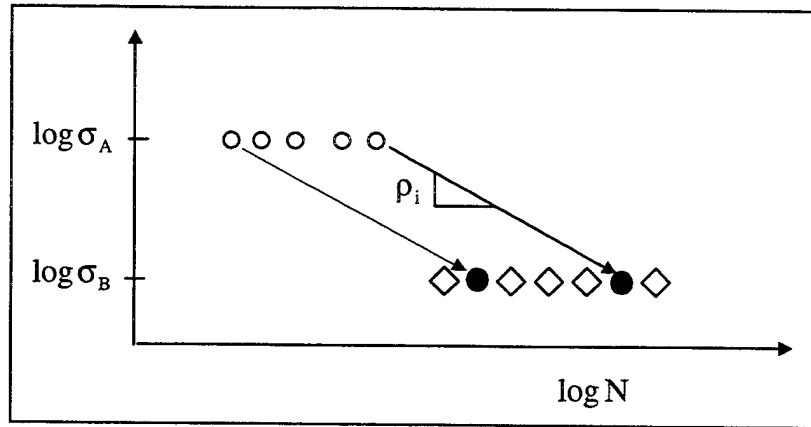


Figure 5.4. Life Transformation Example Illustration

Under the assumption ρ_i is constant, but unknown, for given data sets $\{D_A\}$ and $\{D_B\}$ (i.e., for the same rank), implies the breakdown rules or damage functions are identical. There are many slopes, ρ_i , that can be used. For instance, a very steep slope (almost vertical) would group the data from $\{D_A\}$ to the left of the data in $\{D_B\}$ causing a concentration of the data to be in the lower tail of the merged data sets. On the other hand, if the slope were very shallow, the data would then be concentrated in the upper tail. The goal in this methodology was to find the best slope that corresponds to the least amount of disorder in the merged data set. Therefore it was hypothesized that the maximum shape parameter, $\alpha_{i_{\max}}$, of the merged data set exhibits the least amount of disorder or minimum entropy in the merged data set.

b. Interpretation

The two candidate data sets considered for life transformation into data set $\{D_{3_e}\}$ at the low stress level (data set with the most refined technique) were data sets $\{D_{21}\}$ and $\{D_{14}\}$ at the medium and high stress levels. Because the shape parameter for $\{D_{14}\}$ was considerably larger than the shape parameter at the low stress level (i.e., $\alpha_{14} = 8.9$, $\alpha_{3_e} = 4.8$), this transformation was judged inappropriate because the damage functions for the data sets were apparently different. However, for the data set $\{D_{21}\}$, the shape parameter was less than that of the low stress level (i.e., $\alpha_{21} = 3.1$, $\alpha_{3_e} = 4.8$).

Therefore, this projection was determined to be more appropriate for this life transformation.

c. *Application*

In order to efficiently project the data from data set $\{D_{21}\}$ to $\{D_3\}_e$, a Microsoft EXCEL Worksheet was used with a programmed macro to perform the repeated operations to obtain the merged data sets for a range of slopes. The data set $\{D_{21}\}$ had to first be projected from the medium stress level of 30.9 ksi to the low stress level of 25.6 ksi in the log-log space. The equation used to perform the projection, $N_{f_{21}} \Rightarrow N'_{f_{21}}$, was determined to be;

$$N'_{f_{21}} = \exp(\log N_{f_{21}}) + \frac{1}{\rho_i} (\log \sigma_{a_3} - \log \sigma_{a_2}). \quad (5.6)$$

In this equation, $N_{f_{21}}$ is the observed data in $\{D_{21}\}$ and $N'_{f_{21}}$ denotes the projected data from $\{D_{21}\}$ into $\{D_3\}_e$. The terms σ_{a_3} and σ_{a_2} are the stress amplitudes at the low and medium stress levels, respectively. Once the life transformations were performed, the data was combined with $\{D_3\}_e$, ranked, sorted, and plotted in the weakest link space. An example of a weakest link plot of transformed data is shown in Figure 5.6.

The weakest link plots were used to determine the appropriate range of slopes needed to make the minimum entropy observation mentioned earlier. Projections were performed at various slopes from very large (steep) to very small (shallow) to observe the data clusters at the lower and upper tails in the weakest link plots. These visual observations determined the range of ρ_i to be from -0.04 to -0.06. The resulting data sets were then computed for each ρ_i in this range with an increment of 0.01 resulting in a total of twenty data sets. Each data set was then input as exact data into the MLE software for maximum likelihood parameter analysis. Each $\alpha_{i_{\max}}$ was computed and plotted versus each corresponding slope, ρ_i , as shown in Figure 5.5. The results show that $\rho = -0.05$ provides the life transformation introducing the least amount of entropy or disorder into the data set. Therefore, the projected data set, $\{D'_{21}\}$ becomes,

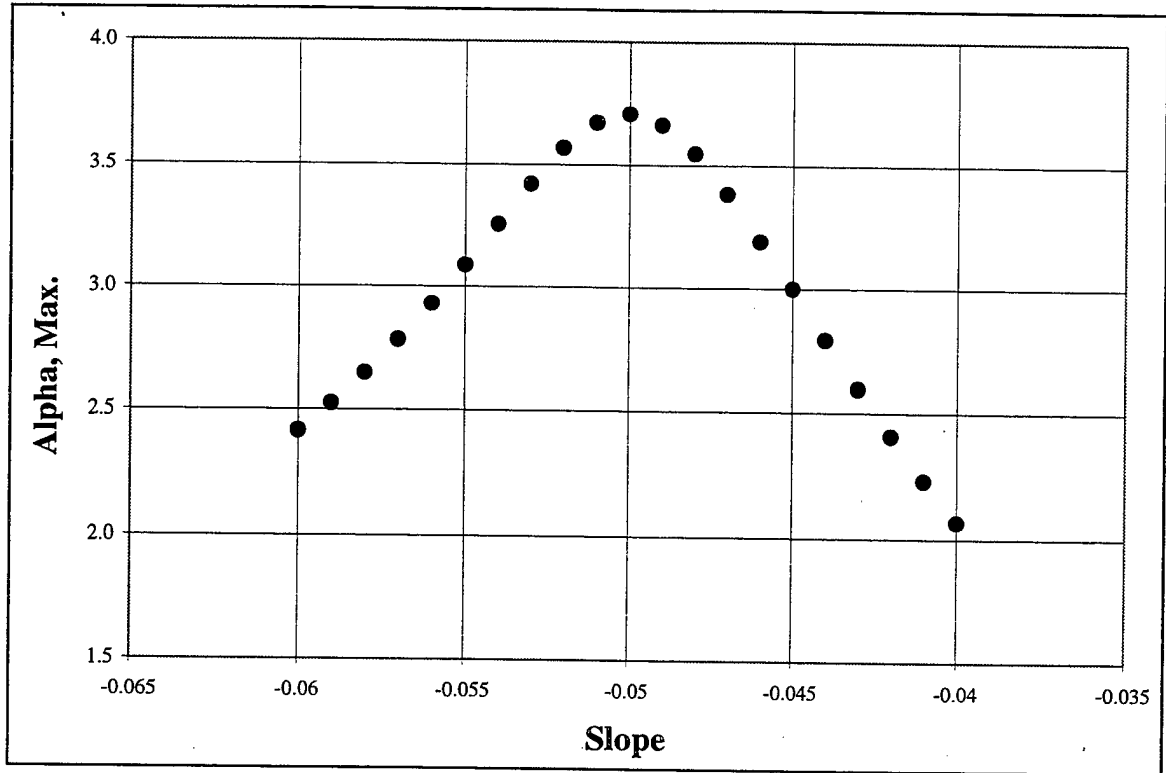


Figure 5.5. α_{\max} vs. ρ_i

$$\{D'_{21}\} = \{D_{21}\}_{\rho=-0.05} \quad (5.7)$$

The resultant data set from combining the projected data with the data set $\{D_{3e}\}$ becomes, $\{D_3\}_{e,p} = \{D_3\}_e \cup \{D'_{21}\}$, where the subscript, p, denotes the inclusion of projected data. The subsequent MLE solution then becomes $\text{MLE } \alpha, \beta | \{D_{33}, D_{34}, D'_{21}\}$, which yielded $\alpha_{3e,p} = 3.7$ and $\beta_{3e,p} = 3.138 \times 10^6$. Figure 5.6 shows the merged data set plotted in the weakest link space. The merged data is denoted as darkened circles. The MLE solution can be found in Appendix B. Both the shape and location parameters decreased slightly. This can be expected due to the greater variability in $\{D_{21}\}$.

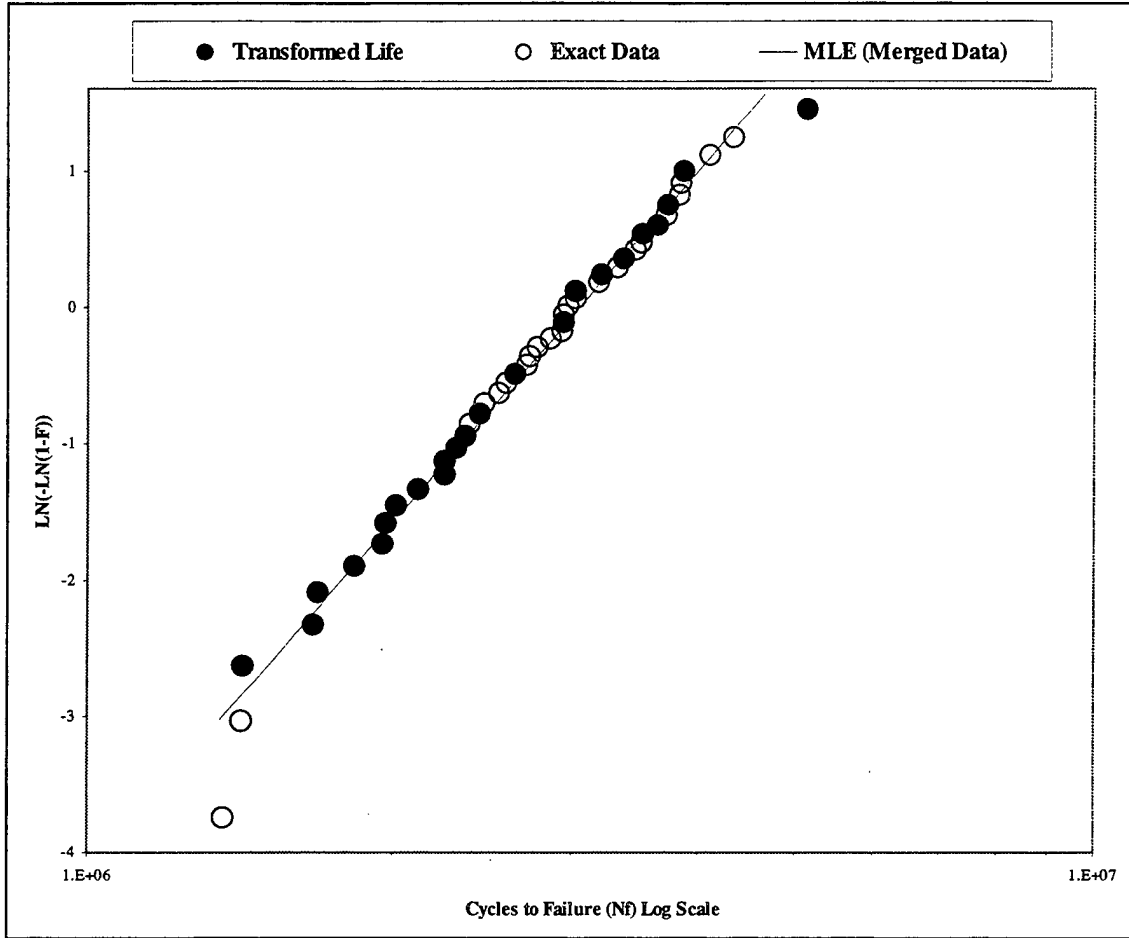


Figure 5.6. $\{D_3\}_{e,p}$ Weakest Link Plot, Merged Data

E. RESULTS OF COMBINED DATA SETS

In summary, the data from the medium and low stress levels was merged by means of equivalent stress level and life (rank is homologous) considerations. The considerations included shape parameter analyses, appropriate data censoring techniques and minimum entropy projection. The final data set is denoted as $\{D_3\}_{e,r,p}$, where the subscripts e, r, and p represent the exact, right censored and projected data, respectively.

The final representation of this data set can be written:

$$\{D_3\}_{e,r,p} = \{D_{34}\} \cup \{D_{33}\} \cup \{D_{31}\}_r \cup \{D_{32}\}_r \cup \{D'_{21}\}_p. \quad (5.8)$$

The results of all of the mentioned merged data sets are summarized in Table 5.3. The table shows the progression of the parameters as each data set was combined. The

important observation to be taken from these results is that the shape and location parameters of the final merged data set were essentially the same as the original data set.

$\{D_{ij}\}$	$\{D_{i1}\}$	$\{D_{i2}\}$	$\{D_{i3}\}$	$\{D_{i4}\}$
$\{D_{1j}\}$				$\alpha_{14} = 8.9$ $\beta_{14} = 1.12 \times 10^4$
$\{D_{2j}\}$	$\alpha_{21} = 3.1$ $\beta_{21} = 6.92 \times 10^4$			
$\{D_{3j}\}$	$\alpha_{31} = 1.5$ $\beta_{31} = 2.42 \times 10^5$	$\alpha_{32} = 1.2$ $\beta_{32} = 1.61 \times 10^6$	$\alpha_{33} = 7.5$ $\beta_{33} = 3.22 \times 10^6$	$\alpha_{34} = 4.2$ $\beta_{34} = 3.29 \times 10^6$
			$\alpha_{3_e} = 4.8$ $\beta_{3_e} = 3.28 \times 10^6$	
	$\alpha_{3_{e,r}} = 5.0$ $\beta_{3_{e,r}} = 3.33 \times 10^6$			
			$\alpha_{3_{e,p}} = 3.7$ $\beta_{3_{e,p}} = 3.14 \times 10^6$	
	$\alpha_{3_{e,r,p}} = 4.1$ $\beta_{3_{e,r,p}} = 3.22 \times 10^6$			

Table 5.3. Combined Data Set Results

For instance, $\alpha_{3e,r,p} \cong \alpha_{34}$ and $\beta_{34} \cong \beta_{3e,r,p}$.

The final data set $\{D_3\}_{e,r,p}$ represents a total of 69 realized data points with 23 exact, 16 right censored, and 23 projected realizations. Therefore it can be safely assumed the shape and location parameters $\alpha = 4.1$ and $\beta = 3.217 \times 10^6$ cycles give a very sound representation of the life distribution parameters for the stress amplitude of $\sigma_a = 25.6$ ksi and amplitude ratio of $R = -1$. Figure 5.7 shows this final data set in the weakest link space with the MLE solutions plotted for both the projected and total combined sets as a comparison.

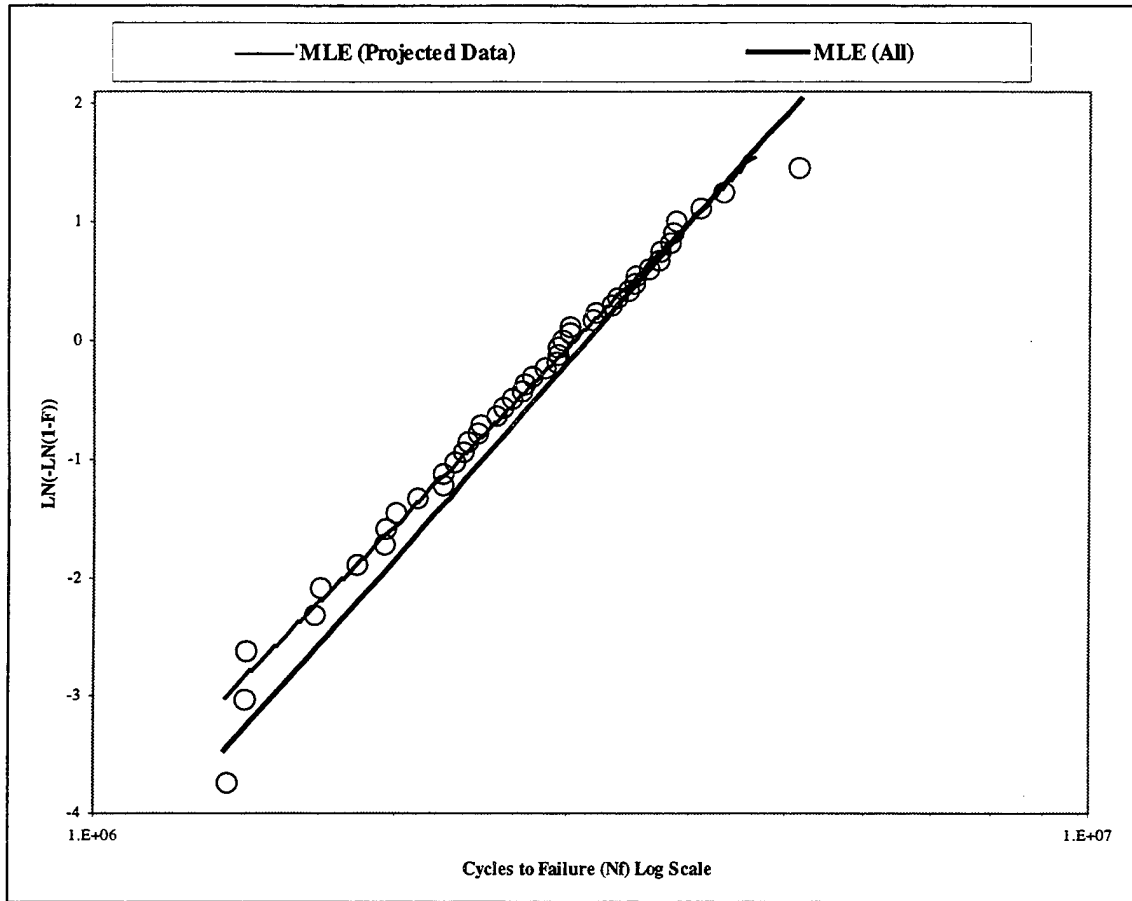


Figure 5.7. $\{D_3\}_{e,r,p}$ Weakest Link Plot

F. FINAL RESULTS

The major efforts of the constant amplitude testing performed for this thesis lie in the testing at the high and low stress levels. The results of the life location and shape parameter for 7075-T6 Aluminum are summarized in Table 5.4.

σ_a (ksi)	α	β
25.6	4.1	3.217×10^6
51.2	8.9	1.122×10^4

Table 5.4. NPS Constant Amplitude Parameters, $R = -1$

The distributions are shown in Figures 5.8 and 5.9. The low stress level life distribution illustrates the importance of the extent of the life variability. The variability

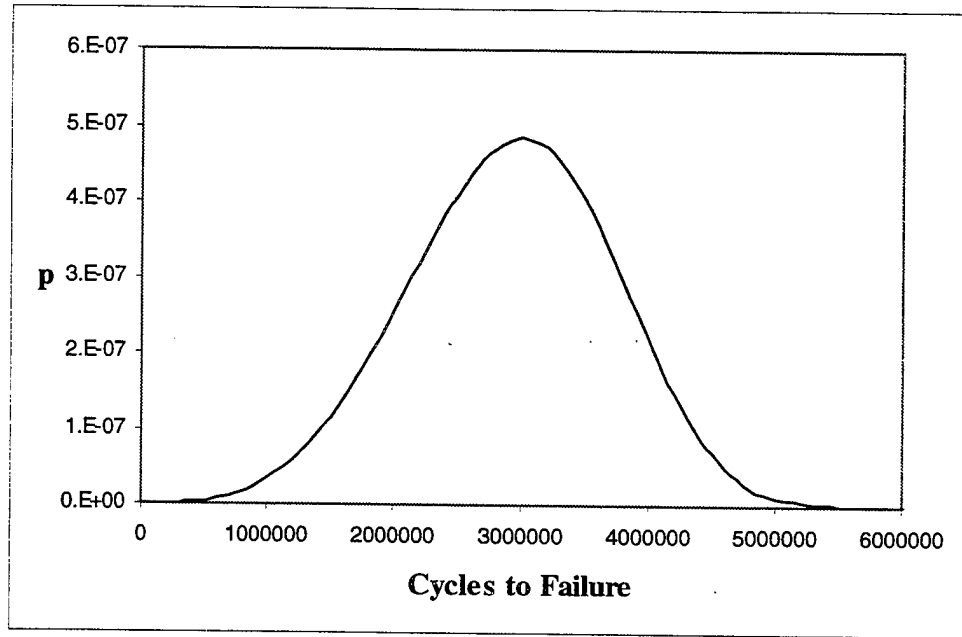


Figure 5.8. Weibull pdf for low stress level data

range is greater than four million cycles. The variability of life in the high stress level distribution shows to be around 10,000 cycles. These observations in life variability again prove the criticality of choice of factor of safety in both cases. For instance, in the low stress amplitude case, the safe life assumption could be approximated to be 600,000 cycles from Figure 5.8. In this case, the factor of safety would have to be

$$\frac{6 \times 10^5}{\beta_{3e,r,p}} = \frac{6 \times 10^5}{3.217 \times 10^6}, \text{ or } 0.19. \text{ Therefore, the factor of safety on life would have to be}$$

5.4 or greater. The same methodology for the high stress amplitude would require the factor of safety on life to be greater than 2.2.

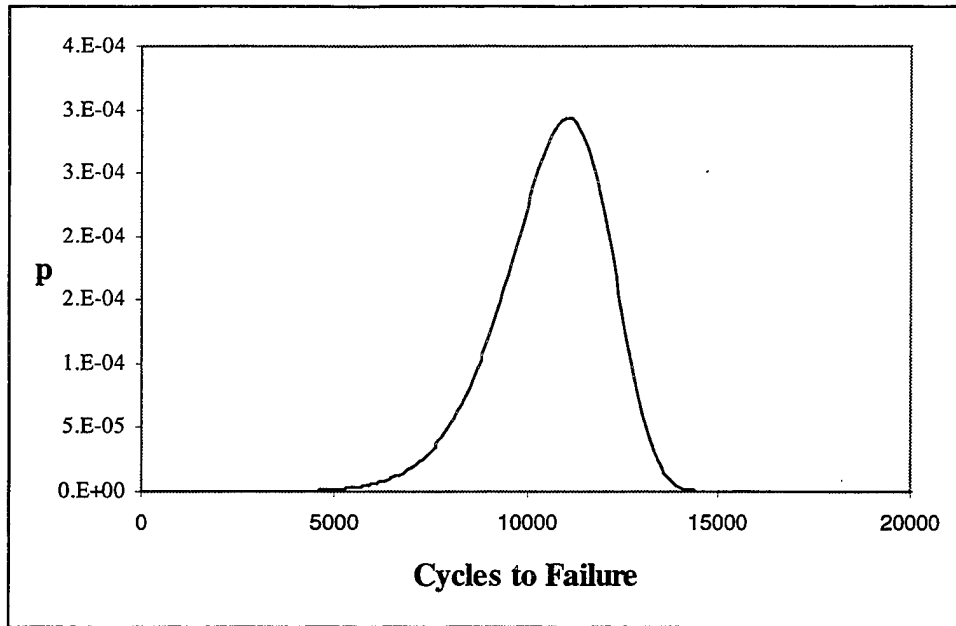


Figure 5.9. Weibull pdf of high stress level data

Hence, the importance of knowing the life location and variability is crucial in making quantified risk and reliability predictions. This information could then be utilized to quantitatively prevent the over or under prediction of the remaining or refurbished structural component safe life remaining.

VI. DAMAGE FUNCTION VISUALIZATION & DATA COMPARISON

Data are frequently presented graphically to test these hypotheses, i.e., whether the trend of data is consistent with the trends of the damage function. These damage function laws have been linearized by semi-log or log-log transformations. The transformations, however, emphasize a certain range of the data and de-emphasize other data ranges. Therefore, it is instructional to view the damage functions in the natural linearized space as well as the non-linearized space.

1. Traditional Methods

These methods have used the exponential and power curve fits to express the damage functions in a more familiar stress-life or S-N curve. Figures 6.1 and 6.2 show

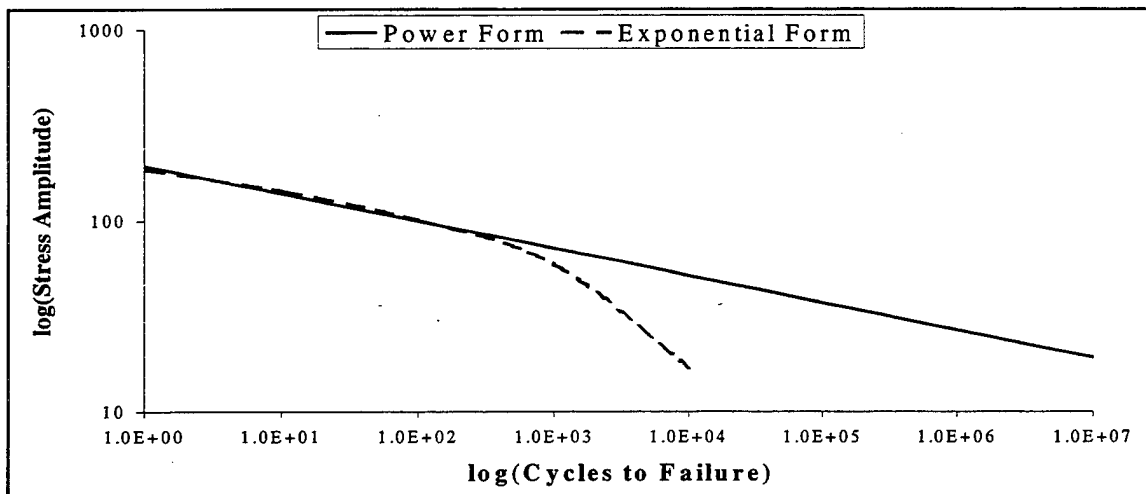


Figure 6.1. Log-Log S-N Curve

each form in the semi-log and log-log space for 7075-T6 Aluminum.

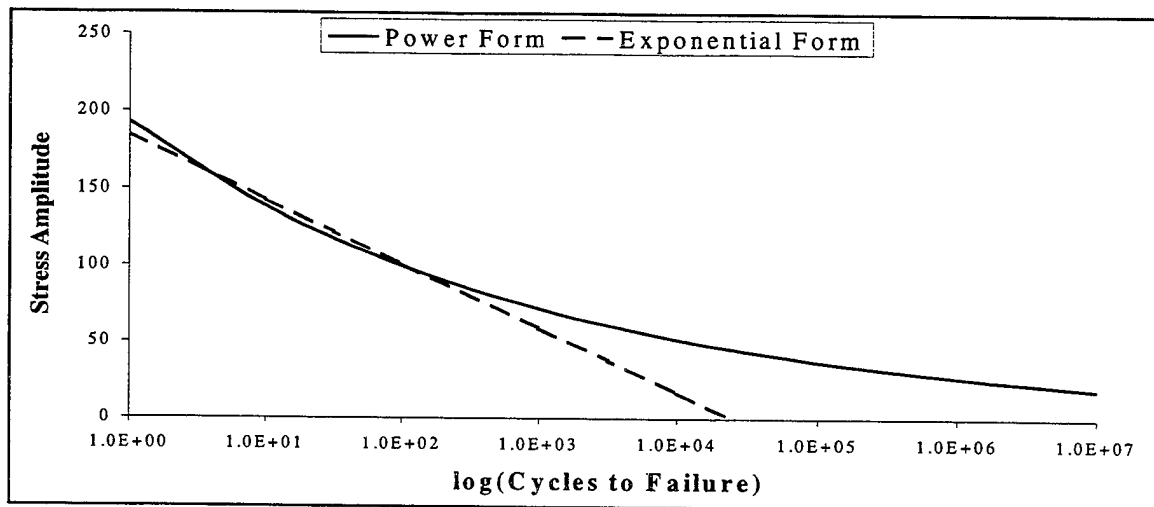


Figure 6.2. Semi-Log S-N Curve

The visualization in the traditional method clearly indicates the general fit of each curve over a specific life range. For instance, the exponential form may indicate a better fit to low cycle fatigue while the power form of these traditional curves may fit high cycle data. The only way of knowing for sure which form of the damage function fits for a certain life cycle range is to compare these curves to experimental data.

B. COMPARISON TO EXPERIMENTAL PUBLISHED DATA

An additional effort to compare the results of the experimentation to published data and damage function forms was also conducted in this investigation. Figure 6.3 contains 7075-T6 Aluminum fatigue data in the log-log space from the data base compiled by LT Todd Kousky[Ref. 5:pp. 47-92] along with additional data from Boller and Seeger[Ref. 6:p.71]. All data plotted in Figure 6.3 were collected under the same constraints with a fully reversed stress amplitude ratio, $R=-1$. Figure 6.4 shows the same set of data in the semi-log space.

The data from testing at the high and low stress levels clearly falls within the published variability at the respective levels. The medium stress testing which was conducted with the analog controller falls somewhat below the values of published data.

The general form of the S-N curve as shown in the log-log space shows a concave downward trend in the low to intermediate cycle range but otherwise it is mostly straight. The curve clearly shows the variability or scatter when multiple fatigue tests are run at

the same stress level. The variability in cycles to failure is also observed to increase with life.

The form of the curve in the semi-log space indicates some slightly different observations. Again the curve appears to be mostly straight but slightly concave up in the high cycle range. The variability appears somewhat more constant in the semi-log space but does open up in the high cycle range similar to the log-log observations.

C. DAMAGE FUNCTION FORM COMPARISONS TO EXPERIMENTAL DATA

If a comparison is made in the log-log space between Figures 6.1 and 6.3, the data in Figure 6.3 indicate the S-N curve is mostly straight with a slight concave downward trend. By the curves in Figure 6.1, this observation would suggest the use of the exponential form of the damage function as a model.

However, if the same comparison were made in the semi-log space, the data in Figure 6.4 indicate the curve is mostly straight with a slight concave upward trend. For this observation Figure 6.2 suggests the power form of the damage function as a model.

Therefore, it is quite evident that the failure mechanisms seem to show a mixture throughout the life cycle ranges being studied in this investigation. Since the failure mechanisms appear to be combined over this life range, a combination of forms of the damage function must be used in the analytical model. Clearly, further experimentation and data collection would have to be done to clarify these observation for a better understanding of the failure mechanisms needed to refine the damage function modeling and formulations.

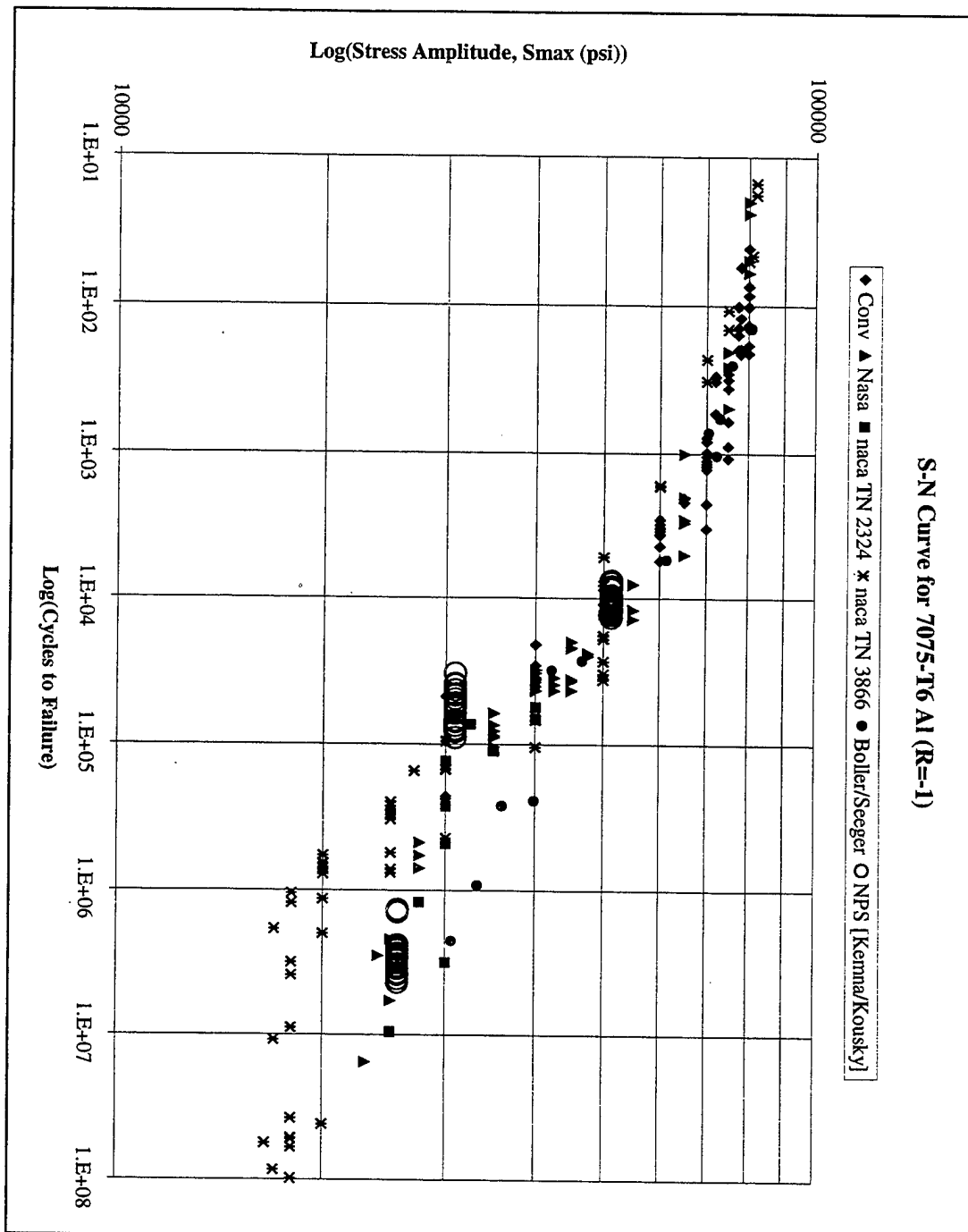


Figure 6.3. NPS Data Comparison Log-Log S-N Curve

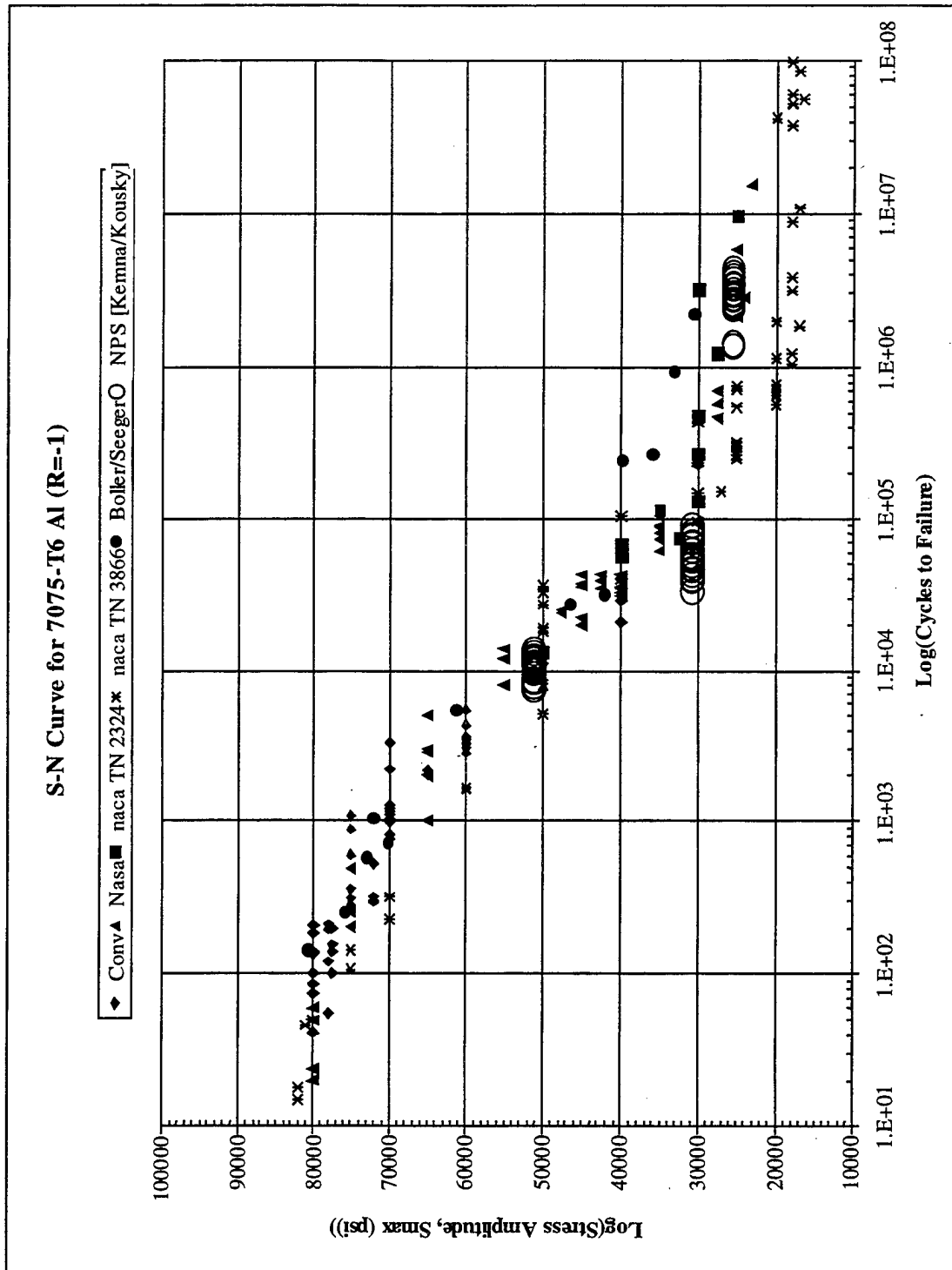


Figure 6.4. NPS Data Comparison Semi-Log S-N Curve

VII. FAILURE MECHANISMS

A. FRACTURE MORPHOLOGY OBSERVATIONS

In order to better observe test validity and associated failure mechanisms, each of the failed specimens were physically arranged in order of increasing fatigue life (i.e., shortest life to the right and longest life to the left). Specimens which had failed outside of the uniform test sections were analyzed as censored data (i.e., the observed life is

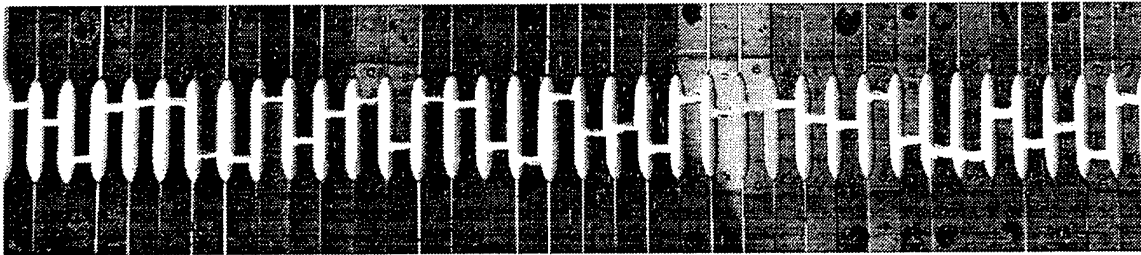


Figure 7.1. High Stress Level Failed Specimens

treated to be less than or equal to the intrinsic life) and were thus excluded from these observations. Figures 7.1 and 7.2 are photos taken of the failed specimens at the high and low stress levels, respectively. Additional photos providing close-up views of these sets

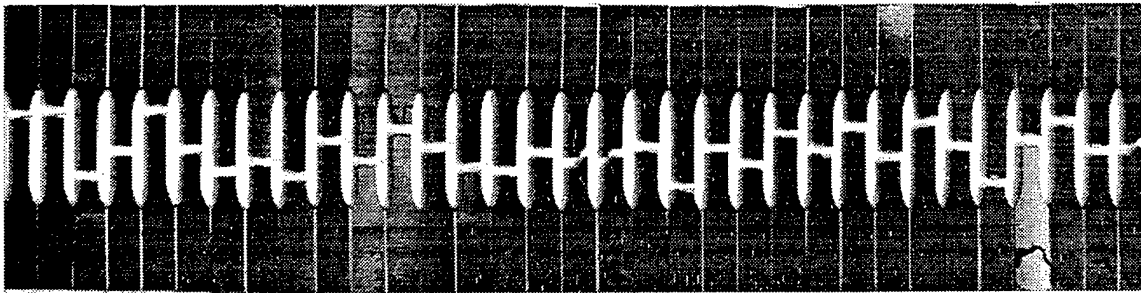


Figure 7.2. Low Stress Level Failed Specimens

of failed specimens can be found in Appendix E.

Fracture morphology is an indicator of the underlying failure mechanism. A plane of failure perpendicular to the direction of the applied load is associated with brittle failure. A plane of failure at an angle of 45 degrees from the direction of applied load is associated with ductile failure. There are two planes of maximum shear; one in the plane of the sample, the other in the plane of the thickness. The ultimate ductile failure

condition may be in either, or, or both of these planes resulting in a tearing appearance. An example of this can best be observed in Figures E.6 or E.7 of Appendix E.

Cursory observations of high stress level failed specimens (resulting in short lives) indicate most of the fracture planes are associated with brittle failure. Low stress level failed specimens (resulting in long lives) are mixed between brittle and ductile failures. Furthermore, the mixture between brittle and ductile failure modes appeared to be random within the range of life observed. These morphological observations suggest that within the range of applied stress, there are two failure mechanisms which take place simultaneously. These mechanisms seemed to be opposite to those surmised in literature. For instance, ductile failure is generally associated with high stress level fatigue.

These observations can only be confirmed with more extensive statistics from more samples tested under carefully controlled conditions. When the failure mechanisms are considered, appropriate damage functions can be formulated to not only correlate the failure data but be consistent with the failure mechanism as well.

VIII. CONSTANT AMPLITUDE FATIGUE TESTING

A. INTRODUCTION

In order to gain a better understanding of the associated failure mechanisms, variability and life location of fatigue test data, a major undertaking in the development of this thesis was to further collect constant amplitude fatigue data.

B. TEST FACILITY & EQUIPMENT

All testing was accomplished on the NPS Aeronautics Series 810 Materials Test System made by the MTS Systems Corporation. This system is made up of three major assemblies consisting of the load frame, hydraulic power supply and system servo controller. This particular system is a single channel type system made up of one hydraulic actuator driven by a single servo-hydraulic control system.

1. Load Frame

The load frame, MTS Model 312.41, is an extremely stiff, standard two-column frame rated at 110 kilo pounds force, kip (50 ton, static) . The frame cross-head is hydraulically actuated and fully adjustable. The cross-head locks are also hydraulically actuated. The load frame assembly consists of five additional components as described below.

a. Hydraulic Actuator

The 204.81 Actuator is double ended and dual acting, specifically designed for the long life requirements of fatigue testing. It is the force-generating and positioning device within the system. A servo valve controls the actuator by porting oil to either side of the piston in response to control signal from the servo controller. The 38.51 square inch piston allows for a six inch stroke of the actuator.

b. Hydraulic Service Manifold

The Model 298.10 Service Manifold is equipped with nitrogen charged accumulators in the service pressure and return lines to ensure proper servo valve operation by smoothing the pressure fluctuation in the hydraulic pressure lines.

c. Force Transducer

The model 661.20E-2 Axial Force Transducer has a fatigue rated capacity of 11 kips. The transducer provides the precision load sensing capability needed for tension-compression fatigue testing.

d. Alignment Fixture

The MTS Model 609 Alignment Fixture gives the ability to ensure proper alignment between the upper and lower grips for more precise test results. This fixture is designed to reduce unwanted bending by improving both the angular and concentric alignment between the grips.

e. Hydraulic Grips

The MTS Model 647.10 Hydraulic Wedge Grips have a fatigue testing capacity rating of 22 kip and have been specifically designed for fatigue testing in MTS servo-hydraulic test systems. The gripping force is adjustable to prevent specimen damage or slippage. Each grip is independently actuated. When actuated, all moving parts are hydraulically locked in place to prevent backlash in full tension and compression testing. The gripping force is constant regardless of test load.

2. Hydraulic Power Supply

The MTS Model 506.20 Hydraulic Power Supply provides a fixed volume fluid power source to the servo-hydraulic testing system by means of an internal gear type pump. The system is capable of providing a constant hydraulic output pressure up to 3000 pounds force per square inch (psi) at a flow rate of 20 gallons per minute (gpm) to the hydraulic actuator via the hydraulic service manifold and servo valve.

3. Servo Controller

The primary function of the servo controller is to develop the error signal used to control the servo hydraulic system while also performing error detection and program pacing. The error signal is further processed to create the desired control signal input as provided to the servo valve which drives the actuator to produce the desired force or position. This signal is processed in proportion to the error signal.

The control signal causes the servo-valve to open in the required direction to minimize the error by porting oil to the correct side of the actuator causing it to stroke and, hence, reduce the deviation or error. When this deviation is zero, the control signal is thus reduced to zero, and the servo-valve assumes a null position. Under dynamic testing, this process operates continuously to minimize the error between commanded and feedback signals.

Over the course of this thesis research and testing, two different servo controllers were utilized. The initial portion of the testing was completed with an MTS analog type servo control system. Through additional funding, this system was replaced with a digital control system made by Schenk Pegasus, which is now Instron-Schenk Technologies.

a. MTS Servo Controller

The Model 442.11 Controller is an electric sub-system containing the principal control, failsafe, and readout selection units in an MTS electro-hydraulic testing system. The entire controller and readout system consisted of several components including the Model 440.13 Servo Controller, 410.31 Digital Function Generator, 413.05 Master Control Panel, 417.01 Counter Panel, 440.14 Valve Driver, 440.21 Transducer Conditioner, 440.31 Feedback Selector, 440.1 Limit Detector, 440.51 Amplitude Measurement Unit and the Tektronics D13 Dual Beam Oscilloscope. The function generator provided the constant amplitude wave shape needed for this testing. The limit detection system provided the necessary fatigue test termination capability.

This controller was utilized for fatigue testing until December 10, 1997. All data collected from tests conducted using this controller have been properly annotated.

b. Schenk Pegasus Constant Amplitude Controller

The Schenk Pegasus (now known as Instron Schenk Technologies or IST) 4900 Single Channel Digital Servo Controller was used to control, measure and monitor the remainder of the fatigue testing for this thesis. It featured Proportional, Integral, Differential and Feedforward (PIDF) digital servo control, AC and DC transducer conditioning, digital inputs and outputs, limit error checking and programmable action lists, file storage for system parameters and an internal function generator. This controller proved to be very useful and integrated nicely with the MTS 810 Materials Test System servo-hydraulic system.

An amplitude control feature was later added and proved to be critical to the constant amplitude fatigue testing being performed. This feature provided the automatic control of the upper and lower stress limits of the stress control fatigue testing. All data collected under this new controller, and under the amplitude control testing, is also properly annotated.

C. EXPERIMENTAL PROCEDURES

1. Test Specimen Description

The Aluminum 7075-T6 test specimens used for the constant amplitude, stress-controlled testing were prepared in 1993. The coupon specimens were cut from four by eight feet sheets which were sheared in the short direction into 0.75 inch strips which were then sheared into six inch bars. Each bar was then machined to meet ASTM Standards as called out for typical flat specimen fatigue testing. The physical layout of the coupons and their dimensions are shown in drawings located in Appendix D. Currently there are 422 coupons left in the NPS P-3 Life Extension Program inventory for future testing.

D. CONSTANT AMPLITUDE FATIGUE TESTING PROCEDURES

Testing at the lower stress amplitude of 25.6 (ksi) was a continuation of testing completed by Kousky[Ref. 5] in 1996. The lower stress amplitude of 25.6 (ksi) was also chosen to study variability effects in the longer life or high cycle fatigue (HCF) regime. The higher stress amplitude of 51.2 (ksi) was chosen to make the same observations in the shorter life, or low cycle fatigue, (LCF) regime. All stress-control tests were done at room temperature.

In order to more accurately study the effects of variability in these regimes, it is of importance to preserve independence and identical distribution among the tests to the maximum extent possible. To do this, extreme care and diligent adherence to testing procedures was performed to make sure each test was done identically to those previous. To facilitate this, specific coupon handling and testing procedures were determined, documented and followed. These procedures are summarized as follows with the exact procedures listed in Appendix C.

1. System Power Up

Procedure 1 of Appendix C dictates proper system power application and complete system warm up. This procedure was documented to foster continuity prior to beginning testing or system tuning.

2. Alignment

In uniaxial testing, perfectly aligned grips produce uniform axial tensile strains in a specimen. For grips to be perfectly aligned, their loading axes must be concentric. Misalignment between the grips produces non-uniform axial strains in a specimen. Some areas will have higher than average strains; other areas will be lower than average. Bending strain is the difference between the average strain and areas with higher or lower than average strains. Therefore it is important to limit the maximum bending strains because they cause specimens to exhibit much lower strengths than if all axial strains were uniform.

The MTS 609 alignment fixture allows these strains to be reduced by improving the concentric and angular alignment. The alignment procedure used to do this can be found in Procedure 2 of Appendix C.

3. Constant Amplitude System Tuning

In a closed loop, servo control system, the controller allows the adjustment of the proportional, integral, differential, and feed forward (PIDF) gains to optimize the servo loop. The controller compares the command signal to the transducer input signal, calculates the error and applies the PIDF gains to the drive signal that controls the servo valve. The tuning function of the Schenk Pegasus controller provides an oscilloscope for viewing the response of the servo loop, while comparing the command and transducer input signals during the adjustment of the loop gain values. The scope can be set up to display a time plot or a cross plot. The steps taken to do this for constant amplitude testing are laid out in Procedure 3 of Appendix C.

4. Coupon Testing Procedures

a. Coupon Preparation

As can be observed in the data of Appendix C, some difficulties were encountered with coupons breaking in the gripping sections. After some research, it was found that the grip teeth were causing localized "stress riser" locations. A coupon preparation procedure was developed to prevent this from occurring without interfering with the fatigue tests. This involved placing small sections of 60 grit Emory cloth between the grips and the gripping sections of the test coupons. The procedure for this coupon preparation technique can be found in Procedure 4a. of Appendix C. This technique proved to be quite successful in preventing any further premature cracking in the gripping sections outside the test sections of the coupons.

b. Force Transducer Zero Suppression

Over time, the force transducer did tend to drift very slightly from three to ten pounds force with no load applied to the upper grip. In order to verify the force

transducer read zero load with no load applied, a zero suppression procedure was written and utilized at the start of each new test. The Schenk Pegasus Controller has a built-in zero suppression function, making this procedure very straight forward. This procedure is annotated in Procedure 4b. of Appendix C.

c. Coupon Installation

The installation procedure for inserting each coupon was also carefully thought out. The gripping process actually induced a relatively small 200 to 300 lbf tension pre-load before the test has started. To minimize this pre-load, a special procedure was established. The maximum pre-load under this procedure is approximately 20 to 30 lbf. This method is described in detail in Procedure 4b. of Appendix C.

d. Servo Valve Balancing

Upon closing the loop of the control system, it was noticed that an additional load offset was also being imparted on the test coupon up to about 40 lbf. The procedure required to zero the offset was centering or "nulling" the servo valve. This method is described in Procedure 4c. of Appendix C.

e. Test Termination & Coupon Removal

Throughout the experimentation phase, it was always important to use extreme caution in recording identical information such as the test configuration for each test performed. The process of removing the coupons and recording the data is described in Procedure 4e. of Appendix C.

IX. CONCLUSIONS & RECOMMENDATIONS

A. CONCLUSIONS

It is clear that fatigue problems continue to play an increasing role in our resource limited environment where the life of current structures has to be fully utilized and even extended. Thus the need to have more definitive techniques for assuring the mechanical integrity of our aging airframe structures and life critical components seems more urgent now than ever. The rework and refurbishment of Sustained Readiness Programs further complicates the life prediction model.

The continuing high level of activity in fatigue related technologies serves to substantiate the criticality of this failure mode in engineering practice. Because of these ongoing efforts, we continue to see notable improvements in both our experimental and computational capabilities and, more frequently, in their productive interplay. Indeed, well-conceived and executed experimentation establishes the dependable database for intelligent model development and also provides the requisite validation tool for fine-tuning newly developed analytical tools.

The NPS Life Extension Program has demonstrated the ability to develop the required analytical model and probabilistic damage function to perform quantified risk assessment. The sensitivity of the data to different operators and equipment was unexpected. For example, the life data from specimens tested by different thesis students indicated significant statistical difference. Even with the same operator, specimens tested with equipment using the two different servo controllers showed significant differences. This calls for the need of sustained support to provide continuity in data generation (for constant amplitude as well as spectrum loading) to completely assess the model.

Chapters VI and VII in this investigation, demonstrated that at least two breakdown rules (damage functions) are required to model the two fatigue failure mechanisms: plastic yielding and elastic crack growth. It was also demonstrated that the two well known breakdown laws (power law and exponential law) will need to be combined (by set theory) to model the life over the practical range of Naval Aviation

applications. This clearly suggests that a set theory formulation of failure mechanisms is an inescapable refinement.

One of the main benefits to Navy fleet aircraft is in the area of reliability. The level of probability of experiencing a failure in a specific structural component on a given aircraft with a known stress history can be determined. A secondary benefit is that readiness can be enhanced through a more accurate determination of the necessary rework required on each aircraft. Therefore, rework and refurbishment efforts in support of sustained readiness programs can be properly assessed and scheduled for each aircraft in lieu of current "full sweep" efforts. The result could lead to significant financial savings while enhancing the safety, readiness, and reliability of our currently aging fleet aircraft.

The fatigue life prediction community can also benefit in that the probabilistic approach adds real value to the contemporary method for predicting the reliability and safety of any structural component. Further development of this modern approach can serve to adequately quantify risk assessment in any structural fatigue situation leading to efficient and effective engineering design.

B. RECOMMENDATIONS

As a result of the experimentation, formulations and research performed in this thesis, the following recommendations for further study are provided:

1. Continue constant amplitude fatigue testing at additional stress levels, R ratios and life ranges to further refine the identification of the damage process and the Boolean formulation of a combined failure mechanism model.
2. Research current fleet spectrum data to conduct spectrum fatigue testing modeling current aircraft mission profiles.
3. Conduct spectrum testing for modified flight profiles and current or proposed payload changes.
4. Test coupon specimens using material cut from refurbished structures with known stress histories (i.e., P-3 Drag Struts) for damage function verification and assessment of safe life remaining.

5. Continue commitment to adequately replace outdated test system components and provide a dedicated laboratory technician to facilitate equipment maintenance and testing continuity. Without these, dependable data is simply not possible.

LIST OF REFERENCES

1. MIL-HDBK-5G, *Fatigue Data Analysis*, vol. 2, pp. 78-130.
2. Coleman., B.D., *Journal of Applied Physics*, vol. 29, pp. 968-983.
3. Phoenix, S.L., and Wu, E.M., "Statistics for the Time Dependent Failure of Kevlar-49 Composites: Micromechanical Modeling and Data Interpretation," *Mechanics of Composite Materials: Recent Advances*. Ed. Zvi Hashin and Carl T. Herakovich. Pergamon Press, 1982, pp. 135-162.
4. Lewis, E.E., *Introduction to Reliability Engineering*, John Wiley & Sons, Inc., 1996.
5. Kousky, T.R., *Conventional and Probabilistic Fatigue Life Prediction Methodologies Relevant to the P-3C Aircraft*, Master's Thesis, Naval Postgraduate School, March 1997.
6. Boller,C. and Seeger,T., *Materials Data For Cyclic Loading. Part D: Aluminum and Titanium Alloys*, Materials Science Monographs, 42D, Elsevier Amsterdam-Oxford-New York-Tokyo, 1987, pp. 69-71.

BIBLIOGRAPHY

- Bannantine, J.A., Cromer, J.J., and Hardroc, J.L., *Fundamentals of Metal Fatigue Analysis*, Prentice-Hall, Inc., 1990.
- Coffin, L.F., "Some Perspectives on Future Directions in Low Cycle Fatigue," *Low Cycle Fatigue*, ASTM STP 942, H. D. Solomon, G.R. Halford, L.R. Kaisand, and B.N. Leis, Eds., American Society for Testing and Materials, Philadelphia, 1988, pp. 5-14.
- Dowling, N.E., *Mechanical Behavior of Materials: Engineering Methods for Deformation, Fracture, and Fatigue*, Prentice-Hall, Inc., 1993.
- Ellyin, Fernand, *Fatigue Damage, Crack Growth and Life Prediction*, Chapman & Hall, 1997.
- Fuchs, H.O., *Metal Fatigue in Engineering*, John Wiley & Sons, Inc., 1980.
- Johnsen, S.E.J. and Doner, M., "A Statistical Simulation Model of Miner's Rule," *Methods for Predicting Material Life in Fatigue*, Ed. W.J. Ostergren and J.R. Whitehead. ASME Winter Annual Meeting, December, 1979, pp. 221-235.
- Landgraf, R.W., Morrow, J.D., and Endo, T., "Determination of the Cyclic Stress-Strain Curve," *Journal of Materials*, JMLSA, Vol. 4, No. 1, March 1969, pp. 176-188.
- Landgraf, R.W., "The Resistance of Metals to Cyclic Deformation," *Achievement of High Fatigue Resistance in Metals and Alloys*, ASTM STP 467, American Society for Testing and Materials, 1970, pp. 3-36.
- Manson, S.S., "Future Directions for Low Cycle Fatigue," *Low Cycle Fatigue*, ASTM STP 942, H.D. Solomon, G.R. Halford, L.R. Kaisand, and B.N. Leis, Eds., American Society for Testing and Materials, Philadelphia, 1988, pp. 15-39.
- Manson, S.S., "Predictive Analysis of Metal Fatigue in the High Cyclic Life Range," *Methods for Predicting Material Life in Fatigue*, Ed. W.J. Ostergren and J.R. Whitehead. ASME Winter Annual Meeting, December, 1979, pp. 145-183.
- Mitchell, M.R., and Landgraf, R.W., Editors, *Advances in Fatigue Lifetime Predictive Techniques: Second Volume*. ASTM STP 1211, American Society for Testing and Materials, Philadelphia, 1993, pp. 1-2.

APPENDIX A. INITIAL DATA INTERPRETATION

The following Tables A-1 through A-6 contain the preliminary data sets described in Chapter IV. Figures A-1 through A-6 are the plots of the data sets in the weakest link space.

High Stress Level Fatigue Data					
Description: NPS(Kemna), Stress Amplitude=51.2 ksi, R=-1, Instron-Schenck Controller, Ampl. Ctrl.					
Specimen No.	N	Sorting		Expected Rank	Weakest Link F*
		Specimen No.	N	n/(N+1)	ln(-ln(1-F))
1	8617	10	7574	0.0270270	-3.597249705
2	11283	5	7804	0.0540541	-2.89011447
3	10699	8	8263	0.0810811	-2.470324827
4	11200	7	8503	0.1081081	-2.167963722
5	7804	1	8617	0.1351351	-1.929767083
6	10481	35	9492	0.1621622	-1.731997102
7	8503	30	9502	0.1891892	-1.561979439
8	8263	34	9769	0.2162162	-1.412137096
9	11309	32	9809	0.2432432	-1.277571256
10	7574	18	9825	0.2702703	-1.154925382
11	10154	15	10120	0.2972973	-1.041793371
12	11906	11	10154	0.3243243	-0.936386078
13	12421	22	10333	0.3513514	-0.837331498
14	10748	21	10457	0.3783784	-0.743548879
15	10120	24	10461	0.4054054	-0.654165997
16	13550	36	10466	0.4324324	-0.568462726
17	11972	6	10481	0.4594595	-0.485831205
18	9825	3	10699	0.4864865	-0.405746748
19	12996	14	10748	0.5135135	-0.327745806
20	10833	20	10833	0.5405405	-0.251408559
21	10457	33	10988	0.5675676	-0.176344427
22	10333	31	11090	0.5945946	-0.102179235
23	11109	23	11109	0.6216216	-0.028542918
24	10461	4	11200	0.6486486	0.044943303
25	12206	26	11272	0.6756757	0.118681532
26	11272	2	11283	0.7027027	0.193115294
27	11630	9	11309	0.7297297	0.26875367
28	11785	27	11630	0.7567568	0.346205667
29	12121	28	11785	0.7837838	0.426232218
30	9502	12	11906	0.8108108	0.509829786
31	11090	17	11972	0.8378378	0.598374
32	9809	29	12121	0.8648649	0.693886907
33	10988	25	12206	0.8918919	0.799587711
34	9769	13	12421	0.9189189	0.921200907
35	9492	19	12996	0.9459459	1.070819877
36	10466	16	13550	0.9729730	1.283962009

Table A- 1. Data Set $\{D_{14}\}$

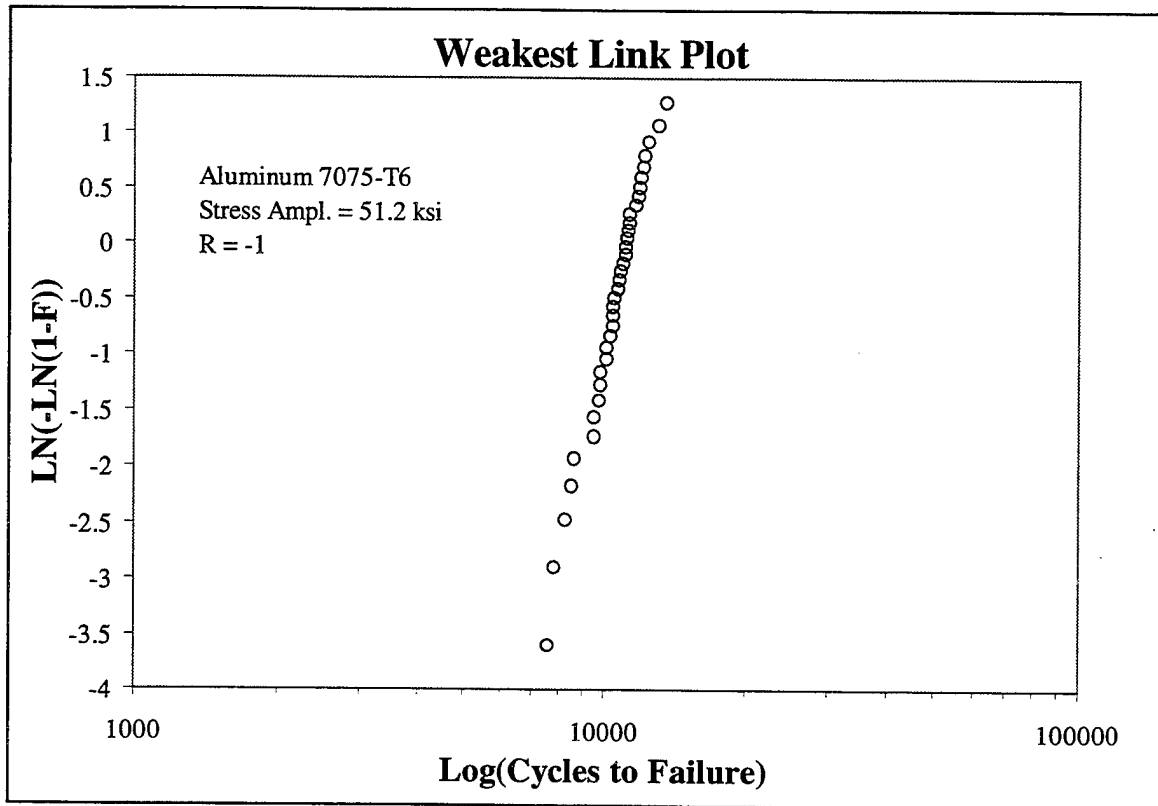


Figure A- 1. $\{D_{14}\}$ Weakest Link Plot

Medium Stress Level Fatigue Data					
Description: NPS(Kousky), Stress Amplitude=30.9 ksi, R=-1, MTS Controller					
Specimen No.		N		Sorting	
Specimen No.		N		Expected Rank	
				Weakest Link F*	
				n/(N+1)	
				ln(-ln(1-F))	
1	32936	1	32936	0.0416667	-3.156849494
2	38653	2	38653	0.0833333	-2.441716399
3	39149	3	39149	0.1250000	-2.013418678
4	42518	4	42518	0.1666667	-1.701983355
5	45330	5	45330	0.2083333	-1.454081455
6	45541	6	45541	0.2500000	-1.245899324
7	46619	7	46619	0.2916667	-1.064673327
8	49060	8	49060	0.3333333	-0.902720456
9	52150	9	52150	0.3750000	-0.755014863
10	52180	10	52180	0.4166667	-0.618046200
11	53535	11	53535	0.4583333	-0.489219929
12	54676	12	54676	0.5000000	-0.366512921
13	56482	13	56482	0.5416667	-0.248258101
14	61247	14	61247	0.5833333	-0.132995836
15	68189	15	68189	0.6250000	-0.019356889
16	70194	16	70194	0.6666667	0.094047828
17	74580	17	74580	0.7083333	0.208755483
18	78456	18	78456	0.7500000	0.326634260
19	81847	19	81847	0.7916667	0.450193650
20	89906	21	84452	0.8333333	0.583198081
21	84452	22	86658	0.8750000	0.732099368
22	86658	20	89906	0.9166667	0.910235093
23	119502	23	119502	0.9583333	1.156269006

Table A- 2. Data Set $\{D_{21}\}$

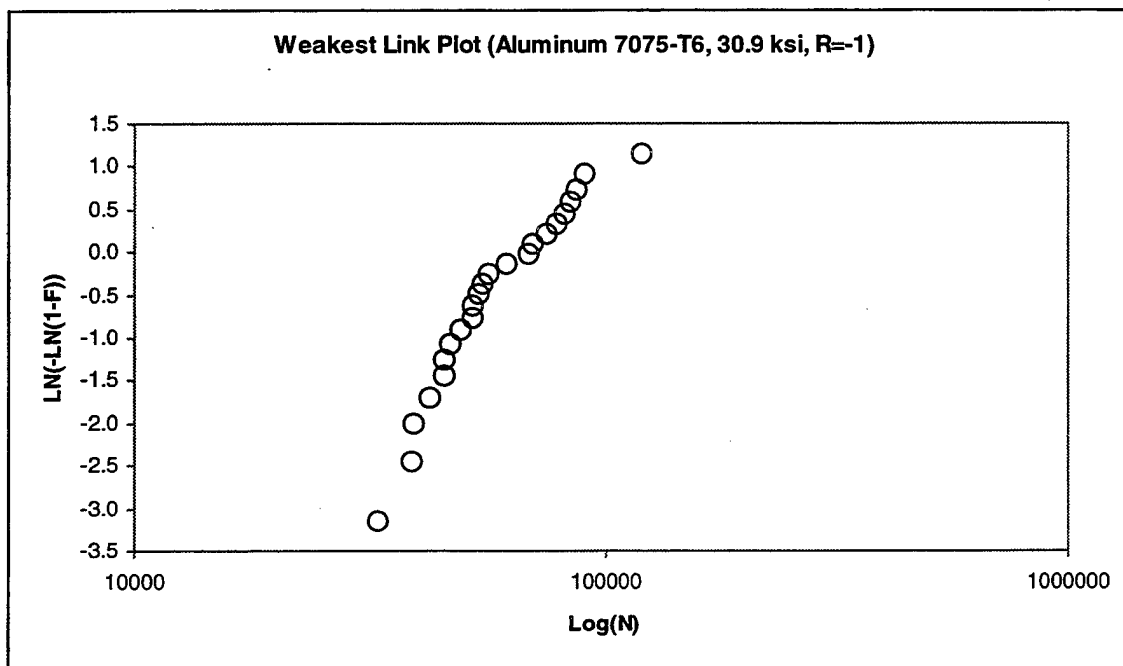


Figure A- 2. $\{D_{21}\}$ Weakest Link Plot

Low Stress Level Fatigue Data					
Description: NPS(Kemna& Kousky), Stress Amplitude=25.6 ksi, MTS, R=-1					
Specimen No.	N	Sorting		Expected Rank	Weakest Link
		Specimen No.	N	$n/(N+1)$	$F^* \ln(-\ln(1-F))$
1	85059	5	83595	0.125	-2.013418678
2	175586	1	85059	0.25	-1.245899324
3	279772	6	110733	0.375	-0.755014863
4	211932	2	175586	0.5	-0.366512921
5	83595	4	211932	0.625	-0.019356889
6	110733	3	279772	0.75	0.32663426
7	561919	7	561919	0.875	0.732099368

Table A- 3. Data Set $\{D_{31}\}$

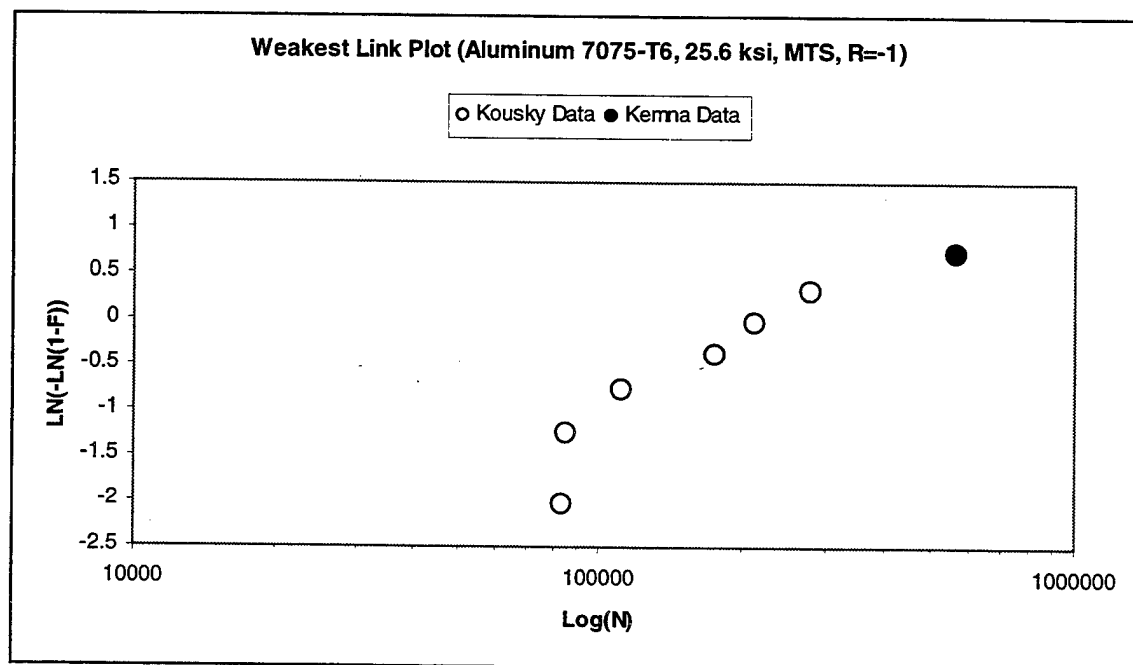


Figure A- 3. $\{D_{31}\}$ Weakest Link Plot

Low Stress Level Fatigue Data					
Description: NPS(Kemna), Stress Amplitude=25.6 ksi, MTS Controller, Emory Cloth Method, R=-1					
Specimen No.		N		Sorting	
Specimen No.		N		Expected Rank	
				Weakest Link F*	
				n/(N+1)	
				ln(-ln(1-F))	
1	862632	4	118074	0.1	-2.250367327
2	2958467	5	346851	0.2	-1.499939987
3	1012679	7	460586	0.3	-1.030930433
4	118074	1	862632	0.4	-0.671726992
5	346851	3	1012679	0.5	-0.366512921
6	2603596	9	2397479	0.6	-0.087421572
7	460586	6	2603596	0.7	0.185626759
8	2828806	8	2828806	0.8	0.475884995
9	2397479	2	2958467	0.9	0.834032445

Table A- 4. Data Set $\{D_{32}\}$

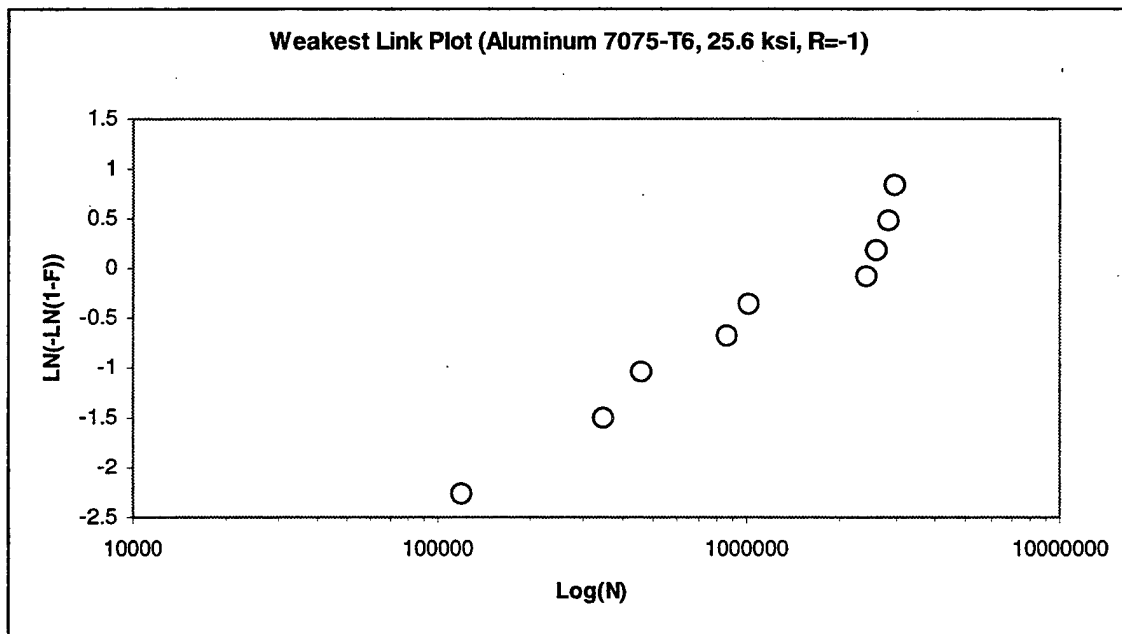


Figure A- 4. $\{D_{32}\}$ Weakest Link Plot

Low Stress Level Fatigue Data					
Description: NPS(Kemna), Stress Amplitude=25.6 ksi, R=-1, Schenck-Pegasus Controller					
Specimen No.		N		Sorting	
Specimen No.		N		Specimen No.	
				Expected Rank	
				Weakest Link F*	
				n/(N+1)	
				ln(-ln(1-F))	
1	2377272	1	2377272	0.1111111	-2.138911028
2	2767101	5	2541395	0.2222222	-1.381050422
3	3720970	4	2722597	0.3333333	-0.902720456
4	2722597	2	2767101	0.4444444	-0.531391212
5	2541395	6	3192715	0.5555556	-0.209573275
6	3192715	8	3333827	0.6666667	0.094047828
7	3514703	7	3514703	0.7777778	0.408179685
8	3333827	3	3720970	0.8888889	0.787195008

Table A- 5. Data Set $\{D_{33}\}$

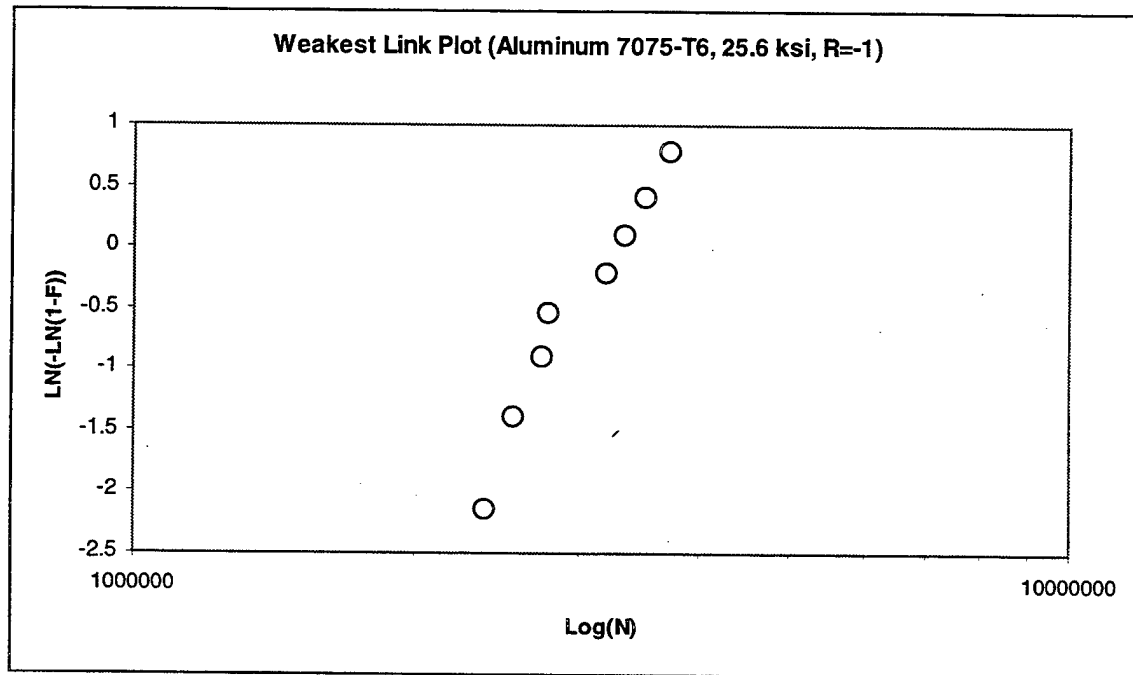


Figure A- 5. $\{D_{33}\}$ Weakest Link Plot

Low Stress Level Fatigue Data					
Description: NPS(Kemna), Stress Amplitude=25.6 ksi, R=-1, Instron-Schenck Controller, Ampl. Ctrl.					
Specimen No.	N	Sorting		Expected Rank	Weakest Link
		Specimen No.	N	$n/(N+1)$	$F^* \ln(-\ln(1-F))$
1	3845245	11	1360949	0.062500	-2.740493007
2	3464846	10	1417504	0.125000	-2.013418678
3	2454992	3	2454992	0.187500	-1.571952527
4	2703580	7	2583897	0.250000	-1.245899324
5	2940130	4	2703580	0.312500	-0.981647055
6	4338783	14	2852160	0.375000	-0.755014863
7	2583897	9	2929710	0.437500	-0.552752143
8	2971067	5	2940130	0.500000	-0.366512921
9	2929710	8	2971067	0.562500	-0.190339326
10	1417504	15	3023503	0.625000	-0.019356889
11	1360949	2	3464846	0.687500	0.151132538
12	4112113	13	3831401	0.750000	0.326634260
13	3831401	1	3845245	0.812500	0.515201894
14	2852160	12	4112113	0.875000	0.732099368
15	3023503	6	4338783	0.937500	1.019781441

Table A- 6. Data Set $\{D_{34}\}$

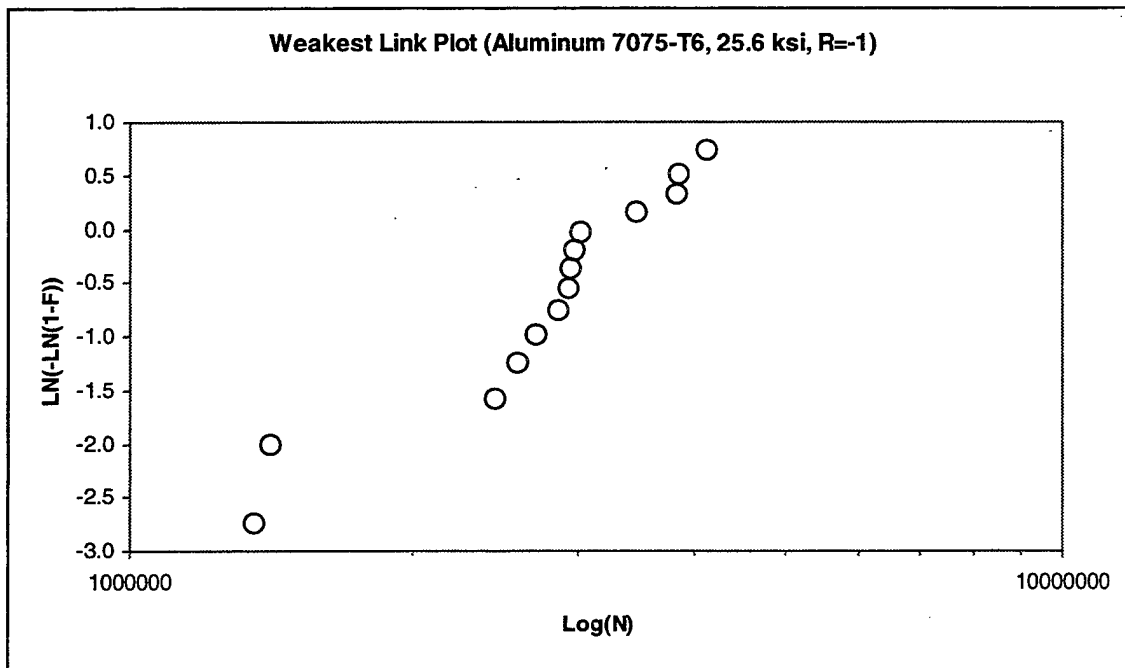


Figure A- 6. $\{D_{34}\}$ Weakest Link Plot

APPENDIX B. MLE PARAMETER SOLUTIONS

The following entries contain the maximum likelihood parameter estimation solutions for each of the data sets as described in Chapters IV and V. The software was written in MATLAB by Prof. E.M. Wu at NPS. The solutions have been downloaded from the Command Window. The parameter solutions are located at the end of each Command Window readout.

$\{D_{14}\}$:

» D14

xe =

8617
11283
10699
11200
7804
10481
8503
8263
11309
7574
10154
11906
12421
10748
10120
13550
11972
9825
12996
10833
10457
10333
11109
10461
12206
11272
11630
11785
12121
9502
11090
9809

```

10988
9769
9492
10466
Total Number of Exact Data points
ne =
36
xr =
[]
xr =
2.2251e-308
Total Number of Right-Censored Data Points
nr =
1
nra =
0
xl =
[]
Total Number of Left-Censored Data Points
nl =
1
nla =
0
Total Number of Data Points
N =
36
least square estimated shape and scale parameters
alpha =
8.4070
beta =
1.1241e+004
Use least-square parameters-estimates to guide...
entering parameter ranges for Likelihood calculation
PRESS ANY KEY TO CONTINUE
Enter the ranges of Weibull Parameters for Likelihood Calculation
Shape Parameter Alpha minimum=3
Shape Parameter Alpha maximum=15
# increments for Alpha=(49)199
Location Parameter Beta minimum=(>0)5000
Location Parameter Beta maximum=25000
# increments for Beta=(49)199
delt_area =
6.0605
wL =
7.4955

```

Underflow may occur indicated by NaN warning (for Large N; change wL to 0

ans =

Total volume under exact Likelihood surface

VLew =

2.4111e-015

Lkemax =

6.6675e-004

ans =

Total volume under Likelihood surface

VL =

1.0000

Lknmax =

6.6675e-004

ans =

MLE Shape and Location of exact sub-set data by calculus

Ae =

8.8823

Be =

1.1220e+004

ans =

MLE Shape and Location of exact and right censored data set by calculus

Aer =

8.8823

Ber =

1.1220e+004

Note that calculus computed MLE coincide with Graphical MLE...

only when data censors are appropriate (no Left censored data).

PRESS ANY KEY to Observe MLE Plot in Weakest Link Space.

Calculus MLE is plotted for exact data in Weakest Link Plot

PRESS ANY KEY TO CONTINUE

Use Lower Right Graph (fig 2) to specify parameter-ranges...

for refining Graphical identification of maximum

Shape Parameter Alpha minimum=8

Shape Parameter Alpha maximum=10

Location Parameter Beta minimum=1.0e4

Location Parameter Beta maximum=1.3e4

From Figure 4, observe Contour maximums for Weakest Link plot of exact data

Press any key to continue

alpha max=8.8823

beta max=11220

$\{D_{21}\}$:

» D21

xe =

32936
38653
39149
42518
45330
45541
46619
49060
52150
52180
53535
54676
56482
61247
68189
70194
74580
78456
81847
84452
86658
89906
119502

Total Number of Exact Data points

ne =

23

xr =

[]

xr =

2.2251e-308

Total Number of Right-Censored Data Points

nr =

1

nra =

0

xl =

[]

Total Number of Left-Censored Data Points

nl =

1

nla =

0

Total Number of Data Points

N =

23

least square estimated shape and scale parameters

alpha =

3.2749

beta =

6.9096e+004

Use least-square parameters-estimates to guide...

entering parameter ranges for Likelihood calculation

PRESS ANY KEY TO CONTINUE

Enter the ranges of Weibull Parameters for Likelihood Calculation

Shape Parameter Alpha minimum=2

Shape Parameter Alpha maximum=6

increments for Alpha=(49)199

Location Parameter Beta minimum=(>0)3e4

Location Parameter Beta maximum=8e4

increments for Beta=(49)199

delt_area =

5.0504

wL =

7.0475

Underflow may occur indicated by NaN warning (for Large N; change wL to 0

ans =

Total volume under exact Likelihood surface

VLew =

1.5608e-039

Lkemax =

7.4007e-005

ans =

Total volume under Likelihood surface

VL =

1.0000

Lknmax =

7.4007e-005

ans =

MLE Shape and Location of exact sub-set data by calculus

Ae =

3.1436

Be =

6.9149e+004

ans =

MLE Shape and Location of exact and right censored data set by calculus

Aer =

3.1436

Ber =

6.9149e+004

Note that calculus computed MLE coincide with Graphical MLE...
only when data censors are appropriate (no Left censored data).
PRESS ANY KEY to Observe MLE Plot in Weakest Link Space.
Calculus MLE is plotted for exact data in Weakest Link Plot
PRESS ANY KEY TO CONTINUE
Use Lower Right Graph (fig 2) to specify parameter-ranges...
for refining Graphical identification of maximum
Shape Parameter Alpha minimum=3
Shape Parameter Alpha maximum=4
Location Parameter Beta minimum=6e4
Location Parameter Beta maximum=7e4
From Figure 4, observe Contour maximums for Weakest Link plot of exact data
Press any key to continue
alpha max=3.1436
beta max=69149

$\{D_{31}\}$:

» D31

xe =

85059
175586
279772
211932
83595
110733
561919

Total Number of Exact Data points

ne =

7

xr =

[]

xr =

2.2251e-308

Total Number of Right-Censored Data Points

nr =

1

nra =

0

xl =

[]

Total Number of Left-Censored Data Points

nl =

```

1
nla =
0
Total Number of Data Points
N =
7
least square estimated shape and scale parameters
alpha =
1.2767
beta =
2.5119e+005
Use least-square parameters-estimates to guide...
entering parameter ranges for Likelihood calculation
PRESS ANY KEY TO CONTINUE
Enter the ranges of Weibull Parameters for Likelihood Calculation
Shape Parameter Alpha minimum=.8
Shape Parameter Alpha maximum=4
# increments for Alpha=(49)199
Location Parameter Beta minimum=(>0)1e5
Location Parameter Beta maximum=4e5
# increments for Beta=(49)199
delt_area =
24.2418
wL =
5.8579
Underflow may occur indicated by NaN warning (for Large N; change wL to 0
ans =
Total volume under exact Likelihood surface
VLew =
1.0604e-017
Lkemax =
6.3670e-006
ans =
Total volume under Likelihood surface
VL =
1.0000
Lknmax =
6.3670e-006
ans =
MLE Shape and Location of exact sub-set data by calculus
Ae =
1.5200
Be =
2.4164e+005
ans =

```

MLE Shape and Location of exact and right censored data set by calculus

Aer =
1.5200

Ber =
2.4164e+005

Note that calculus computed MLE coincide with Graphical MLE...
only when data censors are appropriate (no Left censored data).

PRESS ANY KEY to Observe MLE Plot in Weakest Link Space.

Calculus MLE is plotted for exact data in Weakest Link Plot

PRESS ANY KEY TO CONTINUE

Use Lower Right Graph (fig 2) to specify parameter-ranges...

for refining Graphical identification of maximum

Shape Parameter Alpha minimum=1.3

Shape Parameter Alpha maximum=1.9

Location Parameter Beta minimum=2.3e5

Location Parameter Beta maximum=2.7e5

From Figure 4, observe Contour maximums for Weakest Link plot of exact data

Press any key to continue

alpha max=1.52

beta max=241640

$\{D_{32}\}$:

» D32

xe =

118074

346851

460586

862632

1012679

2397479

2603596

2828806

2958467

Total Number of Exact Data points

ne =

9

xr =

[]

xr =

2.2251e-308

Total Number of Right-Censored Data Points

```

nr =
  1
nra =
  0
xl =
  []
Total Number of Left-Censored Data Points
nl =
  1
nla =
  0
Total Number of Data Points
N =
  9
least square estimated shape and scale parameters
alpha =
  0.8509
beta =
  1.7496e+006
Use least-square parameters-estimates to guide...
entering parameter ranges for Likelihood calculation
PRESS ANY KEY TO CONTINUE
Enter the ranges of Weibull Parameters for Likelihood Calculation
Shape Parameter Alpha minimum=.5
Shape Parameter Alpha maximum=5
# increments for Alpha=(49)199
Location Parameter Beta minimum=(>0)5e5
Location Parameter Beta maximum=2e6
# increments for Beta=(49)199
delt_area =
  170.4502
wL =
  6.1092
Underflow may occur indicated by NaN warning (for Large N; change wL to 0
ans =
Total volume under exact Likelihood surface
VLew =
  1.9652e-030
Lkemax =
  1.5387e-006
ans =
Total volume under Likelihood surface
VL =
  1.0000
Lknmax =

```

1.5387e-006
 ans =
 MLE Shape and Location of exact sub-set data by calculus
 Ae =
 1.2424
 Be =
 1.6132e+006
 ans =
 MLE Shape and Location of exact and right censored data set by calculus
 Aer =
 1.2424
 Ber =
 1.6132e+006
 Note that calculus computed MLE coincide with Graphical MLE...
 only when data censors are appropriate (no Left censored data).
 PRESS ANY KEY to Observe MLE Plot in Weakest Link Space.
 Calculus MLE is plotted for exact data in Weakest Link Plot
 PRESS ANY KEY TO CONTINUE
 Use Lower Right Graph (fig 2) to specify parameter-ranges...
 for refining Graphical identification of maximum
 Shape Parameter Alpha minimum=1
 Shape Parameter Alpha maximum=2
 Location Parameter Beta minimum=1.3e6
 Location Parameter Beta maximum=1.9e6
 From Figure 4, observe Contour maximums for Weakest Link plot of exact data
 Press any key to continue
 alpha max=1.2424
 beta max=1613200

$\{D_{33}\}$:

» D33

xe =

2377272
 2767101
 3720970
 2722597
 2541395
 3192715
 3514703
 3333827

Total Number of Exact Data points

```

ne =
    8
xr =
    []
xr =
    2.2251e-308
Total Number of Right-Censored Data Points
nr =
    1
nra =
    0
xl =
    []
Total Number of Left-Censored Data Points
nl =
    1
nla =
    0
Total Number of Data Points
N =
    8
least square estimated shape and scale parameters
alpha =
    5.8258
beta =
    3.2458e+006
Use least-square parameters-estimates to guide...
entering parameter ranges for Likelihood calculation
PRESS ANY KEY TO CONTINUE
Enter the ranges of Weibull Parameters for Likelihood Calculation
Shape Parameter Alpha minimum=1
Shape Parameter Alpha maximum=10
# increments for Alpha=(49)199
Location Parameter Beta minimum=(>0)1e6
Location Parameter Beta maximum=4e6
# increments for Beta=(49)199
delt_area =
    681.8010
wL =
    5.9915
Underflow may occur indicated by NaN warning (for Large N; change wL to 0
ans =
Total volume under exact Likelihood surface
VLew =
    7.0213e-024

```

```

Lkemax =
  5.4531e-007
ans =
Total volume under Likelihood surface
VL =
  1
Lknmax =
  5.4531e-007
ans =
MLE Shape and Location of exact sub-set data by calculus
Ae =
  7.4975
Be =
  3.2199e+006
ans =
MLE Shape and Location of exact and right censored data set by calculus
Aer =
  7.4975
Ber =
  3.2199e+006
Note that calculus computed MLE coincide with Graphical MLE...
only when data censors are appropriate (no Left censored data).
PRESS ANY KEY to Observe MLE Plot in Weakest Link Space.
Calculus MLE is plotted for exact data in Weakest Link Plot
PRESS ANY KEY TO CONTINUE
Use Lower Right Graph (fig 2) to specify parameter-ranges...
for refining Graphical identification of maximum
Shape Parameter Alpha minimum=7
Shape Parameter Alpha maximum=8
Location Parameter Beta minimum=3e6
Location Parameter Beta maximum=4e6
From Figure 4, observe Contour maximums for Weakest Link plot of exact data
Press any key to continue
alpha max=7.4975
beta max=3219900

```

$\{D_{34}\}$:

```

» D34
xe =
  3845245
  3464846

```

2454992
 2703580
 2940130
 4338783
 2583897
 2971067
 2929710
 1417504
 1360949
 4112113
 3831401
 2852160
 3023503
 Total Number of Exact Data points
 ne =
 15
 xr =
 []
 xr =
 2.2251e-308
 Total Number of Right-Censored Data Points
 nr =
 1
 nra =
 0
 xl =
 []
 Total Number of Left-Censored Data Points
 nl =
 1
 nla =
 0
 Total Number of Data Points
 N =
 15
 least square estimated shape and scale parameters
 alpha =
 2.9844
 beta =
 3.3844e+006
 Use least-square parameters-estimates to guide...
 entering parameter ranges for Likelihood calculation
 PRESS ANY KEY TO CONTINUE
 Enter the ranges of Weibull Parameters for Likelihood Calculation
 Shape Parameter Alpha minimum=1

```

Shape Parameter Alpha maximum=15
# increments for Alpha=(49)199
Location Parameter Beta minimum=(>0)1e6
Location Parameter Beta maximum=5e6
# increments for Beta=(49)199
delt_area =
  1.4141e+003
wL =
  6.6201
Underflow may occur indicated by NaN warning (for Large N; change wL to 0
ans =
Total volume under exact Likelihood surface
VLew =
  1.6691e-049
Lkemax =
  8.7963e-007
ans =
Total volume under Likelihood surface
VL =
  1
Lknmax =
  8.7963e-007
ans =
MLE Shape and Location of exact sub-set data by calculus
Ae =
  4.1784
Be =
  3.2936e+006
ans =
MLE Shape and Location of exact and right censored data set by calculus
Aer =
  4.1784
Ber =
  3.2936e+006
Note that calculus computed MLE coincide with Graphical MLE...
only when data censors are appropriate (no Left censored data).
PRESS ANY KEY to Observe MLE Plot in Weakest Link Space.
Calculus MLE is plotted for exact data in Weakest Link Plot
PRESS ANY KEY TO CONTINUE
Use Lower Right Graph (fig 2) to specify parameter-ranges...
for refining Graphical identification of maximum
Shape Parameter Alpha minimum=4
Shape Parameter Alpha maximum=4.5
Location Parameter Beta minimum=3e6
Location Parameter Beta maximum=3.5e6

```

From Figure 4, observe Contour maximums for Weakest Link plot of exact data

Press any key to continue

alpha max=4.1784

beta max=3.2936e6

$\{D_3\}_e$:

» D3e

xe =

2377272

2767101

3720970

2722597

2541395

3192715

3514703

3333827

3845245

3464846

2454992

2703580

2940130

4338783

2583897

2971067

2929710

1417504

1360949

4112113

3831401

2852160

3023503

Total Number of Exact Data points

ne =

23

xr =

[]

xr =

2.2251e-308

Total Number of Right-Censored Data Points

nr =

1

```

nra =
  0
xl =
[]
Total Number of Left-Censored Data Points
nl =
  1
nla =
  0
Total Number of Data Points
N =
  23
least square estimated shape and scale parameters
alpha =
  3.7131
beta =
  3.3398e+006
Use least-square parameters-estimates to guide...
entering parameter ranges for Likelihood calculation
PRESS ANY KEY TO CONTINUE
Enter the ranges of Weibull Parameters for Likelihood Calculation
Shape Parameter Alpha minimum=1
Shape Parameter Alpha maximum=15
# increments for Alpha=(49)199
Location Parameter Beta minimum=(>0)1e6
Location Parameter Beta maximum=5e6
# increments for Beta=(49)199
delt_area =
  1.4141e+003
wL =
  7.0475
Underflow may occur indicated by NaN warning (for Large N; change wL to 0
ans =
Total volume under exact Likelihood surface
VLew =
  2.5651e-073
Lkemax =
  1.3998e-006
ans =
Total volume under Likelihood surface
VL =
  1.0000
Lknmax =
  1.3998e-006
ans =

```

MLE Shape and Location of exact sub-set data by calculus

Ae =

4.7925

Be =

3.2756e+006

ans =

MLE Shape and Location of exact and right censored data set by calculus

Aer =

4.7925

Ber =

3.2756e+006

Note that calculus computed MLE coincide with Graphical MLE...

only when data censors are appropriate (no Left censored data).

PRESS ANY KEY to Observe MLE Plot in Weakest Link Space.

Calculus MLE is plotted for exact data in Weakest Link Plot

PRESS ANY KEY TO CONTINUE

Use Lower Right Graph (fig 2) to specify parameter-ranges...

for refining Graphical identification of maximum

Shape Parameter Alpha minimum=4.5

Shape Parameter Alpha maximum=5

Location Parameter Beta minimum=3e6

Location Parameter Beta maximum=3.5e6

From Figure 4, observe Contour maximums for Weakest Link plot of exact data

Press any key to continue

alpha max=4.7925

beta max=3.2756e6

$$\underline{\{D_3\}_{e,r} :}$$

» D3er

xe =

2377272

2767101

3720970

2722597

2541395

3192715

3514703

3333827

3845245

3464846

2454992

2703580
2940130
4338783
2583897
2971067
2929710
1417504
1360949
4112113
3831401
2852160
3023503

Total Number of Exact Data points

ne =

23

xr =

85059
175586
279772
211932
83595
110733
561919
118074
346851
460586
862632
1012679
2397479
2603596
2828806
2958467

xr =

1.0e+006 *

0.0000
0.0851
0.1756
0.2798
0.2119
0.0836
0.1107
0.5619
0.1181
0.3469
0.4606

```

0.8626
1.0127
2.3975
2.6036
2.8288
2.9585
Total Number of Right-Censored Data Points
nr =
  17
nra =
  16
xl =
  []
Total Number of Left-Censored Data Points
nl =
  1
nla =
  0
Total Number of Data Points
N =
  39
least square estimated shape and scale parameters
alpha =
  3.1371
beta =
  4.3298e+006
Use least-square parameters-estimates to guide...
entering parameter ranges for Likelihood calculation
PRESS ANY KEY TO CONTINUE
Enter the ranges of Weibull Parameters for Likelihood Calculation
Shape Parameter Alpha minimum=1
Shape Parameter Alpha maximum=15
# increments for Alpha=(49)199
Location Parameter Beta minimum=(>0)1e6
Location Parameter Beta maximum=5e6
# increments for Beta=(49)199
delt_area =
  1.4141e+003
wL =
  7.0475
Underflow may occur indicated by NaN warning (for Large N; change wL to 0
ans =
Total volume under exact Likelihood surface
VLew =
  2.5651e-073

```

```

Lkemax =
  1.3998e-006
ans =
Total volume under Likelihood surface
VL =
  0.2057
Lknmax =
  1.4237e-006
ans =
MLE Shape and Location of exact sub-set data by calculus
Ae =
  4.7925
Be =
  3.2756e+006
ans =
MLE Shape and Location of exact and right censored data set by calculus
Aer =
  5.0397
Ber =
  3.3332e+006
Note that calculus computed MLE coincide with Graphical MLE...
only when data censors are appropriate (no Left censored data).
PRESS ANY KEY to Observe MLE Plot in Weakest Link Space.
Calculus MLE is plotted for exact data in Weakest Link Plot
PRESS ANY KEY TO CONTINUE
Use Lower Right Graph (fig 2) to specify parameter-ranges...
for refining Graphical identification of maximum
Shape Parameter Alpha minimum=4.5
Shape Parameter Alpha maximum=5.5
Location Parameter Beta minimum=3.1e6
Location Parameter Beta maximum=3.5e6
From Figure 4, observe Contour maximums for Weakest Link plot of exact data
Press any key to continue
alpha max=5.0397
beta max=3.3332e6

```

$$\underline{\{D_3\}_{e,p}} :$$

```

» D3ep
xe =
  1360949
  1417504

```

1419192
1665534
1686906
1832074
1953242
1962334
2008784
2113965
2247111
2248404
2306790
2355955
2377272
2433775
2454992
2541395
2583897
2639095
2703580
2722597
2767101
2852160
2929710
2938222
2940130
2971067
3023503
3024616
3192715
3213606
3333827
3380621
3464846
3514703
3526737
3638985
3720970
3734040
3831401
3845245
3873994
4112113
4338783
5149268

Total Number of Exact Data points

```

ne =
  46
xr =
  []
xr =
  2.2251e-308
Total Number of Right-Censored Data Points
nr =
  1
nra =
  0
xl =
  []
Total Number of Left-Censored Data Points
nl =
  1
nla =
  0
Total Number of Data Points
N =
  46
least square estimated shape and scale parameters
alpha =
  3.7328
beta =
  3.1367e+006
Use least-square parameters-estimates to guide...
entering parameter ranges for Likelihood calculation
PRESS ANY KEY TO CONTINUE
Enter the ranges of Weibull Parameters for Likelihood Calculation
Shape Parameter Alpha minimum=1
Shape Parameter Alpha maximum=15
# increments for Alpha=(49)199
Location Parameter Beta minimum=(>0)1e6
Location Parameter Beta maximum=5e6
# increments for Beta=(49)199
delt_area =
  1.4141e+003
wL =
  7.7407
Underflow may occur indicated by NaN warning (for Large N; change wL to 0
ans =
Total volume under exact Likelihood surface
VLew =
  3.6385e-141

```

```

Lkemax =
  3.0613e-006
ans =
Total volume under Likelihood surface
VL =
  1.0000
Lknmax =
  3.0613e-006
ans =
MLE Shape and Location of exact sub-set data by calculus
Ae =
  3.7084
Be =
  3.1381e+006
ans =
MLE Shape and Location of exact and right censored data set by calculus
Aer =
  3.7084
Ber =
  3.1381e+006
Note that calculus computed MLE coincide with Graphical MLE...
only when data censors are appropriate (no Left censored data).
PRESS ANY KEY to Observe MLE Plot in Weakest Link Space.
Calculus MLE is plotted for exact data in Weakest Link Plot
PRESS ANY KEY TO CONTINUE
Use Lower Right Graph (fig 2) to specify parameter-ranges...
for refining Graphical identification of maximum
Shape Parameter Alpha minimum=3.5
Shape Parameter Alpha maximum=4
Location Parameter Beta minimum=3e6
Location Parameter Beta maximum=3.3e6
From Figure 4, observe Contour maximums for Weakest Link plot of exact data
Press any key to continue
alpha max=3.7084
beta max=3.1381e6

```

$$\underline{\{D_3\}_{e,r,p} :}$$

```

» D3erp
xe =
  2377272
  2767101

```

3720970
2722597
2541395
3192715
3514703
3333827
3845245
3464846
2454992
2703580
2940130
4338783
2583897
2971067
2929710
1417504
1360949
4112113
3831401
2852160
3023503
1360949
1417504
1419192
1665534
1686906
1832074
1953242
1962334
2008784
2113965
2247111
2248404
2306790
2355955
2377272
2433775
2454992
2541395
2583897
2639095
2703580
2722597
2767101
2852160

2929710
2938222
2940130
2971067
3023503
3024616
3192715
3213606
3333827
3380621
3464846
3514703
3526737
3638985
3720970
3734040
3831401
3845245
3873994
4112113
4338783
5149268

Total Number of Exact Data points

ne =

69

xr =

85059
175586
279772
211932
83595
110733
561919
118074
346851
460586
862632
1012679
2397479
2603596
2828806
2958467

xr =

1.0e+006 *
0.0000

```

0.0851
0.1756
0.2798
0.2119
0.0836
0.1107
0.5619
0.1181
0.3469
0.4606
0.8626
1.0127
2.3975
2.6036
2.8288
2.9585
Total Number of Right-Censored Data Points
nr =
  17
nra =
  16
xl =
[]
Total Number of Left-Censored Data Points
nl =
  1
nla =
  0
Total Number of Data Points
N =
  85
least square estimated shape and scale parameters
alpha =
  3.5155
beta =
  3.5723e+006
Use least-square parameters-estimates to guide...
entering parameter ranges for Likelihood calculation
PRESS ANY KEY TO CONTINUE
Enter the ranges of Weibull Parameters for Likelihood Calculation
Shape Parameter Alpha minimum=1
Shape Parameter Alpha maximum=15
# increments for Alpha=(49)199
Location Parameter Beta minimum=(>0)1e6
Location Parameter Beta maximum=5e6

```

```

# increments for Beta=(49)199
delt_area =
  1.4141e+003
wL =
  8.1461
Underflow may occur indicated by NaN warning (for Large N; change wL to 0
ans =
Total volume under exact Likelihood surface
VLew =
  4.5691e-201
Lkemax =
  4.4805e-006
ans =
Total volume under Likelihood surface
VL =
  0.1223
Lknmax =
  4.4939e-006
ans =
MLE Shape and Location of exact sub-set data by calculus
Ae =
  3.9825
Be =
  3.1867e+006
ans =
MLE Shape and Location of exact and right censored data set by calculus
Aer =
  4.0566
Ber =
  3.2171e+006
Note that calculus computed MLE coincide with Graphical MLE...
only when data censors are appropriate (no Left censored data).
PRESS ANY KEY to Observe MLE Plot in Weakest Link Space.
Calculus MLE is plotted for exact data in Weakest Link Plot
PRESS ANY KEY TO CONTINUE
Use Lower Right Graph (fig 2) to specify parameter-ranges...
for refining Graphical identification of maximum
Shape Parameter Alpha minimum=3.5
Shape Parameter Alpha maximum=4.5
Location Parameter Beta minimum=3e6
Location Parameter Beta maximum=3.5e6
From Figure 4, observe Contour maximums for Weakest Link plot of exact data
Press any key to continue
alpha max=4.0566
beta max=3.2171e6

```


APPENDIX C. NPS CONSTANT AMPLITUDE FATIGUE TEST PROCEDURES

1. SYSTEM POWER & WARM UP PROCEDURE

a. Hydraulic Power Supply (Pump Room)

- 1) Turn on the main electrical power to the hydraulic service system which will also turn on the heat exchanger system and cooling towers.
- 2) This switch is located on the left just inside the door of the pump room.
- 3) If there is no power to this room, check circuit breaker panels P480 and P6.
- 4) Turn on the pump room ventilation fans.
- 5) Check the status of the high pressure filter delta "p".

b. Schenk Pegasus Controller

- 1) Perform a system safety and area situational awareness check while ensuring the crush zone is clear.
- 2) Note the control mode of the controller to make sure it is in the desired mode (POS).
- 3) Check the limit status by noting which parameter are currently in override for safety purposes.
- 4) The system is now ready to go to LOW PRESSURE

CAUTION: Do not use PUMP ON to go to turn the hydraulic system on.

CRUSH ZONE CAUTION: The area under the cross-head and above/around the actuator is a hazardous crush zone. Ensure body parts and objects remain in safe areas. Wear safety goggles and use the provided pointer, insertion clamp, and positioning mirror for obvious safety reasons.

- 5) Press HYD LOW to go to low pressure.
- 6) The hydraulic pump will engage in the low pressure mode.
- 7) Check to see that the system is in position control.
- 8) Wait a few seconds for the system to stabilize and prepare to go to high pressure.
- 9) Press HYD HIGH.
- 10) The hydraulic pump is now operating in the high pressure mode. Allow the system to warm up for approximately 30 minutes for system stabilization.

2. GRIP ALIGNMENT PROCEDURE

- 1) Conduct the system power-up procedure (Procedure 1).
- 2) Use the rigid alignment specimen (steel bar).
- 3) The alignment specimen should be marked left, right, top, and bottom.
- 4) This specimen is of similar length dimensions to simulate test coupons for accuracy.
- 5) Position the lower grip at the actual coupon testing position of – 2.095 inches.
- 6) Refer to the coupon installation procedures if needed.
- 7) Adjust the grip pressure to approximately 500 (psi) to suppress grip teeth indentations
- 8) Insert the rigid alignment specimen in the top grip and close the grip.
- 9) Ensure the specimen is aligned as an actual test coupon.
- 10) Insert a hardened rod (drill rod) in the lower grip.
- 11) The diameter of the rod should be approximately 0.010 (in) greater than the width of the rigid alignment specimen.
- 12) Slowly close the lower grip on the rod without touching the alignment specimen.
- 13) Measure and record the spacing on each side of the alignment specimen.
- 14) Repeat the steps above in each of the geometric configurations to assess the angular and concentric adjustment needed.
- 15) Adjust the alignment fixture accordingly if needed.

3. SYSTEM TUNING PROCEDURE

- 1) Follow the power up procedure and allow the system to warm up.
- 2) Follow the coupon installation procedures and insert a sample coupon to simulate an exact test coupon.
- 3) Select the proper STATIC and SPAN loads, function wave shape and frequency to be used for the actual tests to be performed.
- 4) Ensure amplitude control (AMPL CTRL) is engaged.
- 5) Select DYN START to start the tuning process.
- 6) Go to the TUNING/DRV SIG page.
- 7) Select MANUAL PID TUNING.
- 8) Select MORE INFO.
- 9) Select CROSSPLOT CONT and press ENTR.
- 10) Select STD INFO.
- 11) Observe the tuning crossplot.

- 12) Adjust the PIDF gains as necessary to suppress any loopholes or non-linearity of the crossplot line. The line should be at 45 degrees for a sinusoidal wave form.
- 13) Once the system is tuned, record and save the settings in the SAVE page to ensure all tests will be performed under these PIDF settings.

4. **CONSTANT AMPLITUDE COUPON TESTING PROCEDURES**

a. **Coupon Preparation**

- 1) Cut a $\frac{3}{4}$ inch strip of 60 grit Emory cloth into 1.5 inch lengths.
- 2) Use rubber cement or weather-strip adhesive to attach the Emory cloth sections to the gripping sections of the test coupon with the abrasive side to the coupon.
 - a) Application of a small amount at the far end of the gripping section away from the test section is sufficient since the purpose is only to hold the sections in place for safe coupon insertion.
- 3) Allow the adhesive to set. This should only take ten to fifteen minutes.

b. **Coupon Installation**

- 1) Power up the system and allow to warm up.
- 2) Set the lower grip position in the testing position.
- 3) From the OPR page ensure the system is in POS control.
- 4) Select STATIC and press ENTR.
- 5) Perform a safety check in preparation to move the lower grip.
- 6) Enter -2.095 in. and press ENTR.
 - a) The lower grip should move to the selected position.
 - b) Allow a 10 to 20 seconds for the grip to settle into position.
 - c) Ensure the POS FEEDBACK value reads -2.095 in.
- 7) The lower grip should now be in position ready for installation.
- 8) Insert the coupon for testing.
 - d) Grasp the coupon with the special insertion clamp.
 - e) Place the coupon against the right side of the grips.
 - f) Vertically align the coupon against the guides.
 - g) Vertically position the coupon using an extension mirror.
 - h) Align the bottom of the upper coupon gripping section with the bottom face of the upper alignment guide.
 - i) Close the top grip slowly.
- 9) The coupon should now be in position and ready for closing the bottom grip.

- j) Closing the bottom grip closes the loop of the control system.
- 10) From the OPR page, prepare the system for a control mode switch from POS control to LOAD control.
- k) Check to ensure the STATIC position still reads -2.095 in.
- 11) Select MODE (F12).
 - l) The cursor will now be blinking on LOAD control indicating the system is prepared to go to LOAD control.
- 12) Close the lower grip slowly but without touching the coupon.
- 13) Press ENTR.
- 14) The system will ask "Are you sure?"
- 15) Press ENTR and close the lower grip simultaneously.
- 16) The system is now in LOAD control and the control loop is closed for servo valve balancing and testing.

c. Servo Valve Balancing

- 1) From the OPR page select STATIC.
- 2) Enter 0 and press ENTR.
- 3) Observe the LOAD FEEDBACK.
- 4) If the LOAD FEEDBACK does not indicate approximately 0 the valve will need to be balanced.
- 5) Select TUNING/DRV SIG (F4).
- 6) Select MORE INFO (F5).
- 7) Place the cursor on the VALVE BALANCE value.
- 8) If the LOAD FEEDBACK value is (+) this value will need to be more negative.
- 9) If the LOAD FEEDBACK value is (-) this value will need to be more positive.
- 10) Enter the proper adjustment needed.
- 11) Select OPR(F1).
- 12) Observe the LOAD FEEDBACK value.
- 13) Repeat these steps until the LOAD FEEDBACK value indicates approximately zero.

d. Test Initiation

- 1) Procedures 4(a-c) have been completed.
- 2) From the OPR page check the following:
 - a) Ensure LOAD control and AMPL CTRL are selected.
 - m) Ensure the STATIC value is correct (0 for R=-1).
 - n) Ensure the SPAN value is correct (max. load value).
 - o) Ensure the proper FCTN GEN shape is selected (sine wave).

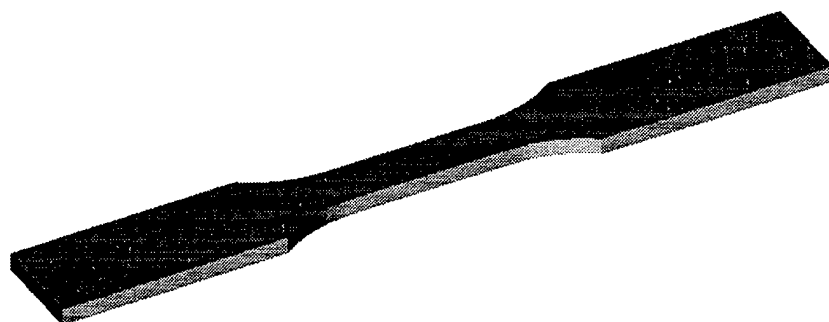
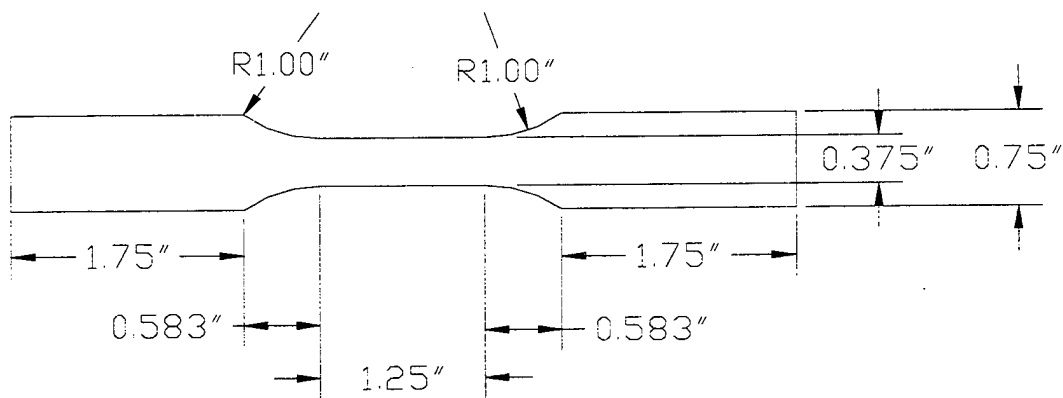
- p) Ensure the correct FREQ is selected (5 Hz).
- q) Ensure the proper visualization windows are set. (i.e. CYCLE AND TOTAL CURRENT COUNT, LOAD FEEDBACK (UPPER/LOWER PEAK), and POS FEEDBACK (UPPER/LOWER PEAK))
- 3) From the LIMIT/DIG IO page perform the following:
 - a) Select VALUES(F12).
 - a) Reset the cycle counters to zero.
 - b) In the CYCLE COUNT position select RESTART and press ENTR.
 - c) In the TOTAL COUNT position select RESTART and press ENTR.
 - d) Ensure every parameter is in OVR except ERROR.
- 4) The system should now be ready to begin testing.
- 5) Check the OPR page for the following items once again:
 - a) Check that AMPL CTRL is indicated.
 - b) Check the STATIC and SPAN values.
- 6) Begin testing by pressing DYN START.
- 7) The system has now begun constant amplitude fatigue testing.
- 8) Allow the system to stabilize.
- 9) Observe the LOAD FEEDBACK(UPPER/LOWER PEAK) values.
 - a) Ensure these values are within the constraints of the test.
- 10) Perform the following to set and arm the limit detection system:
 - a) Select the LIMIT/DIG IO page.
 - b) Select VALUES (F12).
 - c) Select ERROR and set the limit at +/- 7%.
 - d) Select under/over LOAD PEAK and set the limit at +/- 40% of full span.
 - e) Select POSITION and set the limits at +/- 0.05 inches from the peak values.
 - f) Select LOAD and set the limits at +/- 15% of the peak loads.
 - g) Reset any errors (*) that may be indicated for each limit detection category. (Put the cursor on the * and press ENTR.)
 - h) If the error does not reset, the limit may not be entered correctly.
 - i) Reenter the limit and repeat.
- 11) The limit detection system should now be ready to be armed.
- 12) Select OVR ALL (F10).
- 13) This will completely arm the limit detection system.

c. **Test Termination**

- 1) Observe that the test coupon has broken, the hydraulic system has shut down, and the lower grip has settled down to the lowest position.
- 2) Record the pump time.
- 3) Record the number of cycles on the OPR page.
- 4) OVR the errors on the LIMIT/DIG IO page.
 - r) Select OVR ALL (F10).
- 5) From the OPR page switch to POS control.
 - s) Select MODE.
 - t) Select POS and press ENTR.
 - u) The prompt will state "Are you sure?"
 - v) Press ENTR.
- 6) The system is now in POS control to prevent the lower grip from moving.
- 7) Conduct the system power up procedure.
- 8) Release the grips to remove the coupon pieces with clamp.
- 9) Mark the coupon pieces with the appropriate identification.
- 10) Record the appropriate information in the data base.

APPENDIX D. SPECIMEN DRAWINGS

NPS[Kemna, 1998 & Kousky, 1997]



APPENDIX E. FAILED SPECIMEN PHOTOS

Figure E.1 shows the failed specimens at the high stress level. The specimens are shown in the order of life (i.e., shortest life on the left).

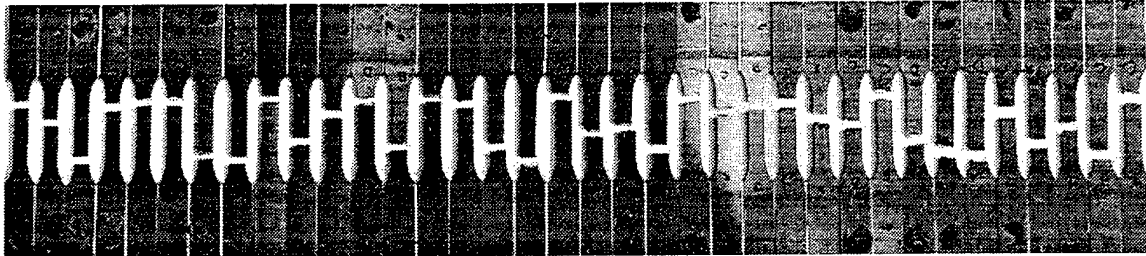


Figure E.1. $\{D_{14}\}$ Failed Specimens

Figure E.2 depicts 33 of 39 failed specimens for the low stress level data in order of life. These are the specimens collected under this thesis investigation.

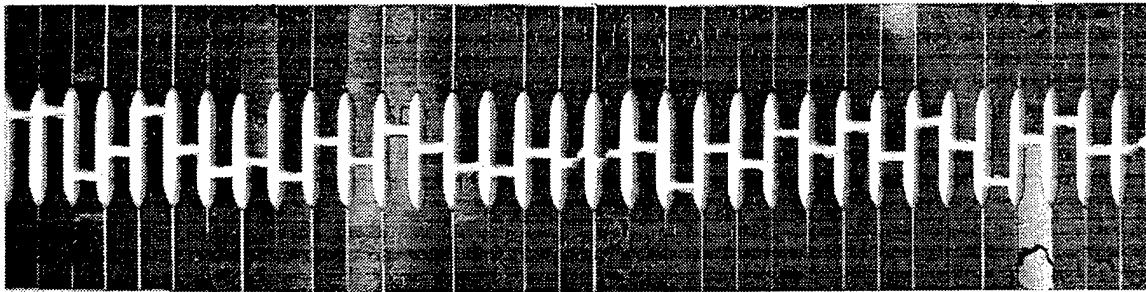


Figure E.2. $\{D_3\}$ Failed Specimens

Figures E.3 and E.4 are close up views of the first 12 specimens and the last 12 specimens, respectively in Figure E.1.

Figures E.5 through E.7 give close-up views of all of the specimens shown in Figure E.2.

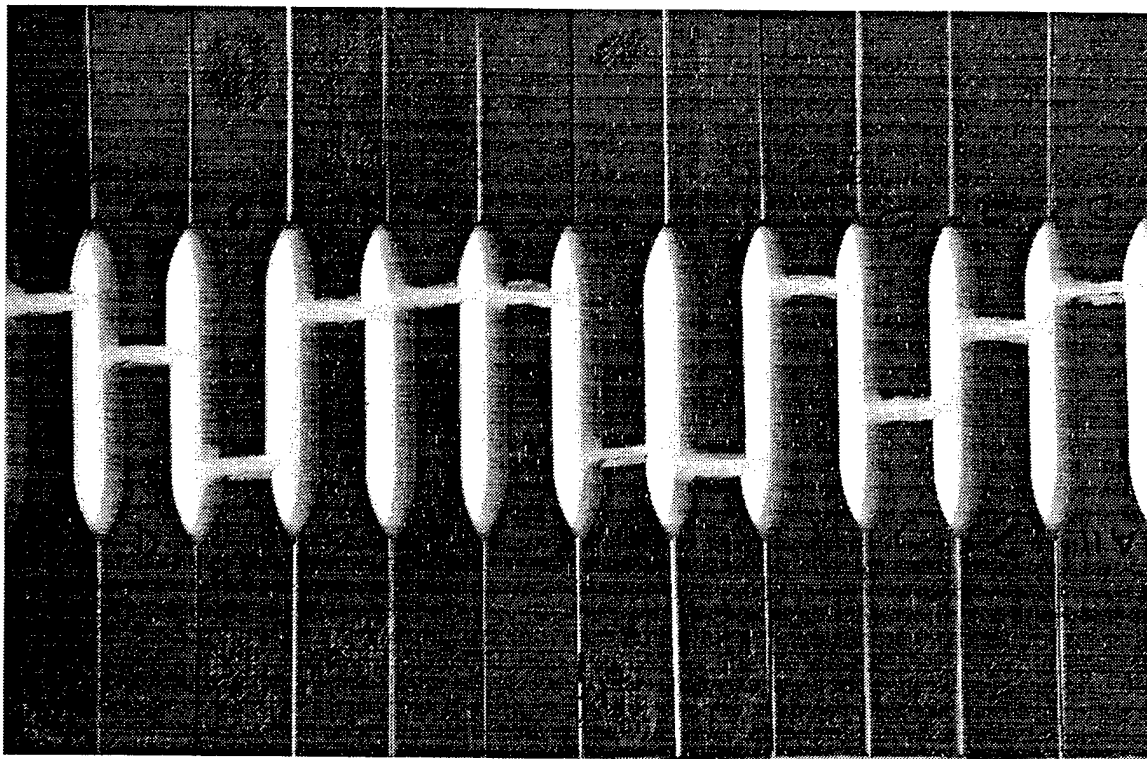


Figure E.3. $\{D_{14}\}$ First 12 Specimens (Lowest Life)

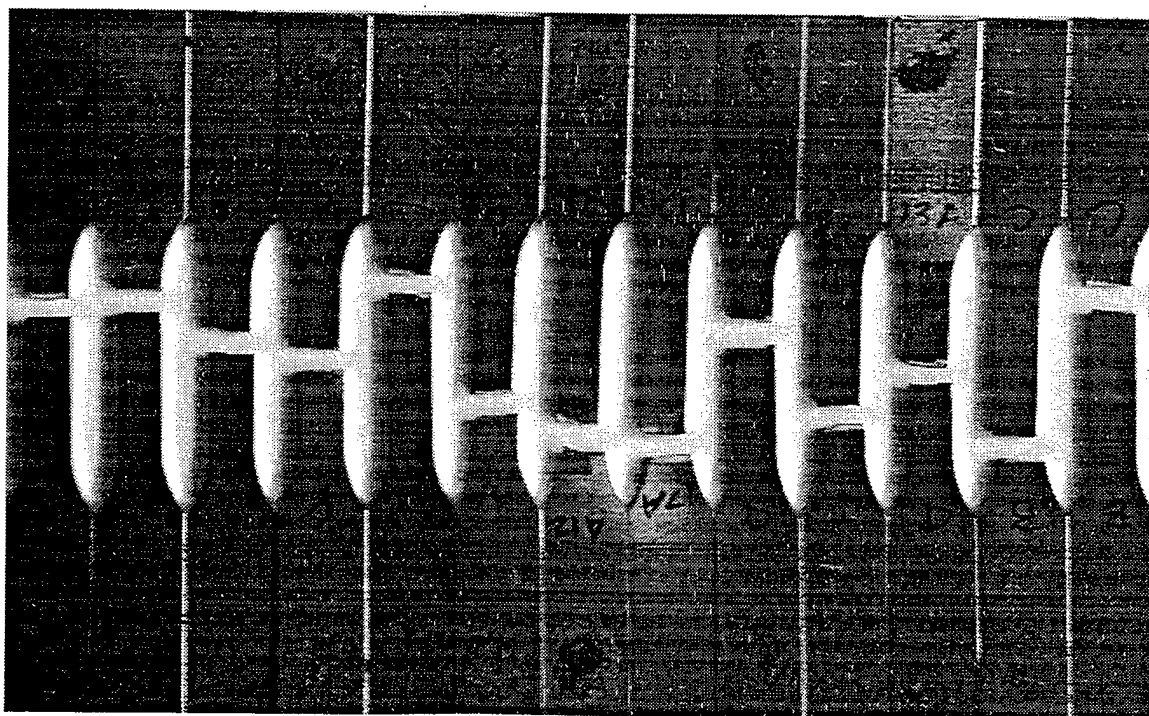


Figure E.4. $\{D_{14}\}$ Last 12 Specimens (Highest Life)

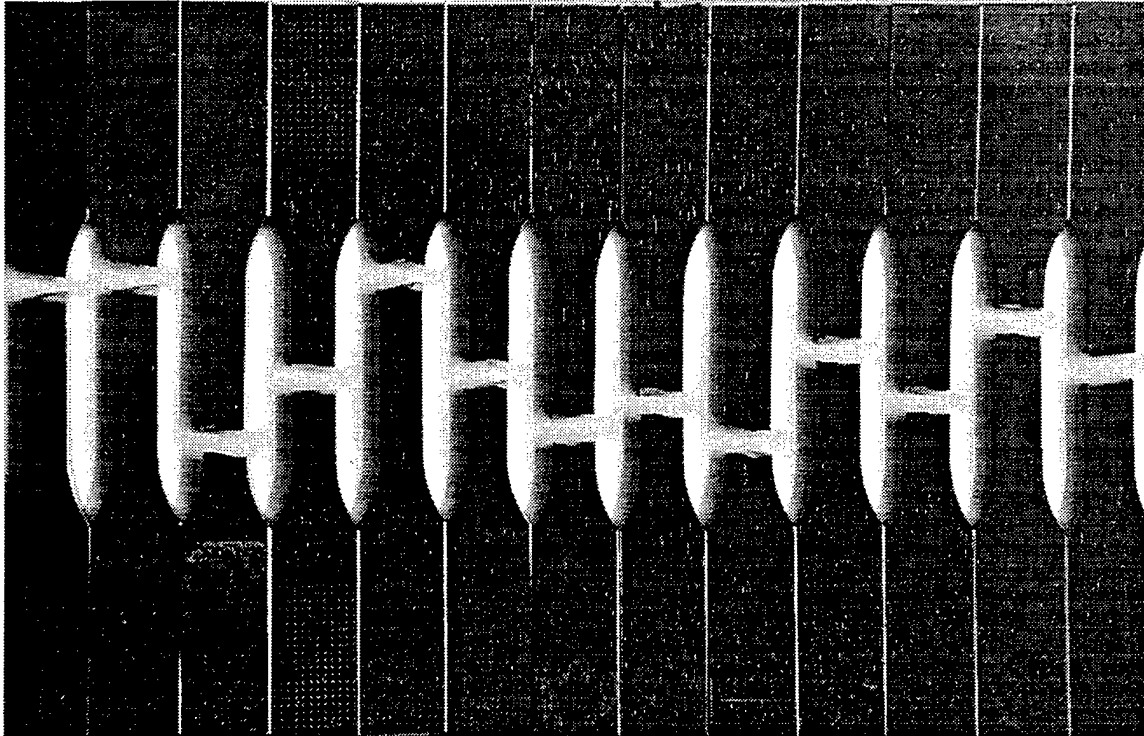


Figure E.5. Low Stress Level, First 13 Failed Specimens

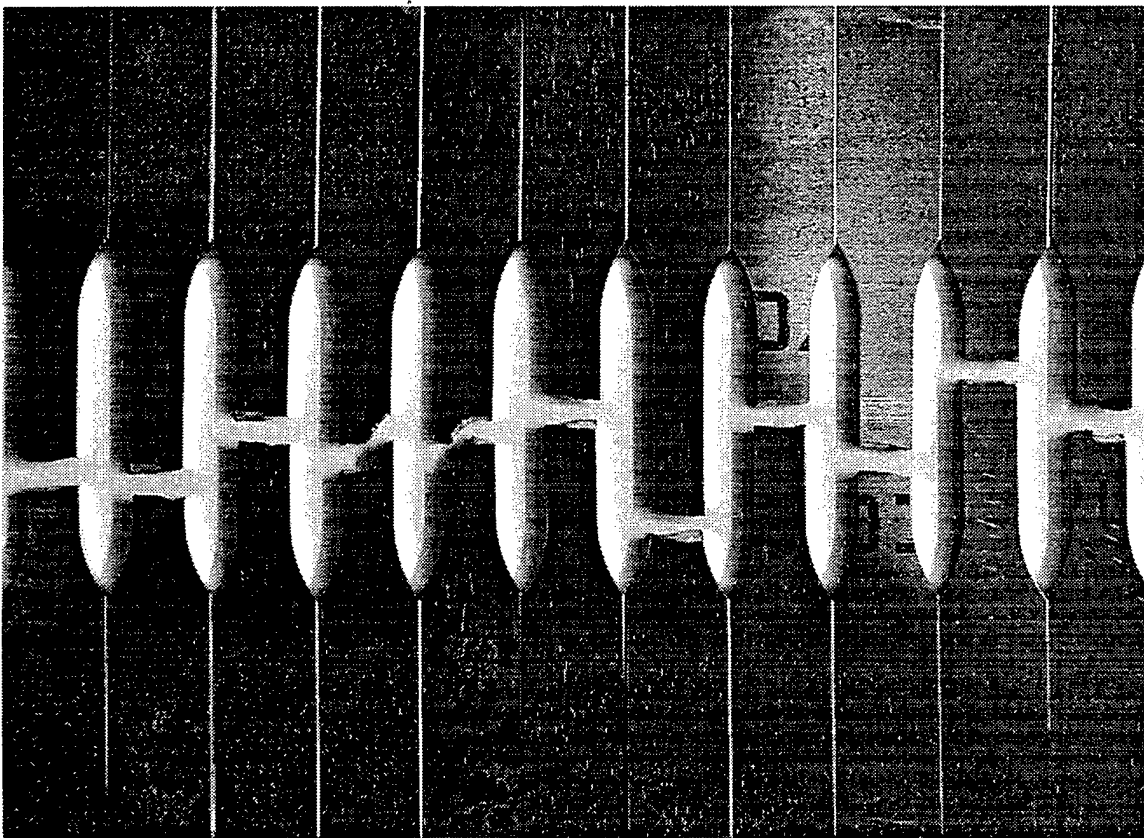


Figure E.6. Low Stress Level, Specimens 14 through 24

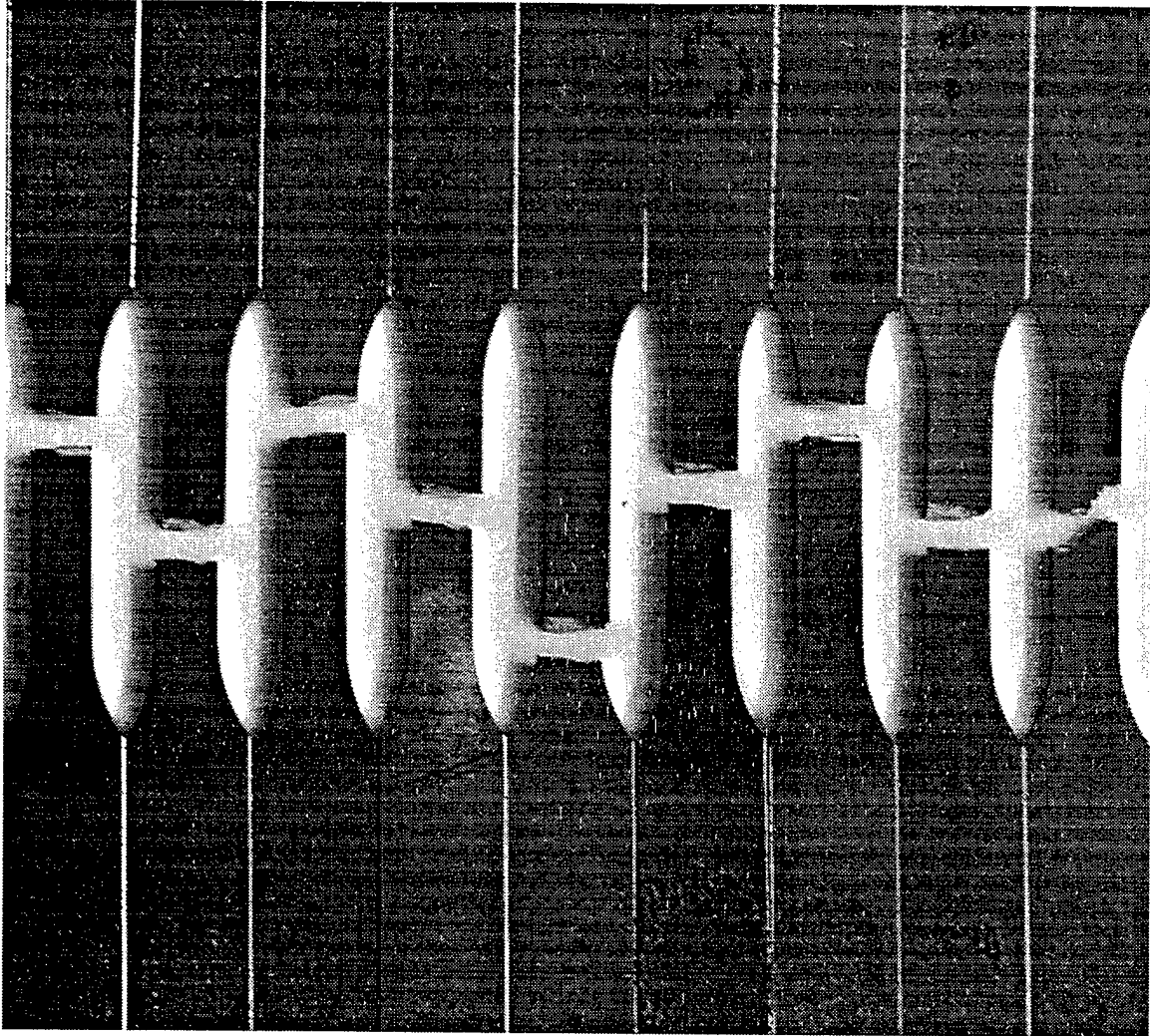


Figure E.7. Low Stress Level, Last 9 Failed Specimens

INITIAL DISTRIBUTION LIST

1. Defense Technical Information Center 2
 8725 John J. Kingman Rd., Suite 0944
 Ft. Belvoir, VA 22060-6218

2. Dudley Knox Library 2
 Naval Postgraduate School
 411 Dyer Rd.
 Monterey, CA 93943-5101

3. Commander, Naval Air Systems Command (AIR-4.1.1.3) 1
 Attn: Mr. Nam D. Phan
 47123 Buse Rd., Bldg. 2272
 Patuxent River, MD 20670

4. Commander, Naval Air Systems Command (PMA-290)..... 1
 Attn: P-3 Class Desk Officer
 47123 Buse Rd., Bldg. 2272, Rm. 146
 Patuxent River, MD 20670

5. Prof. Gerald H. Lindsey, Code AA/Li..... 1
 Chairman, Department of Aeronautics and Astronautics
 Naval Postgraduate School
 Monterey, CA 93943-5000

6. Prof. Edward M. Wu, Code AA/Wu 3
 Department of Aeronautics and Astronautics
 Naval Postgraduate School
 Monterey, CA 93943-5000

7. Lieutenant John G. Kemna..... 1
 600 East 71st Terrace
 Kansas City, MO 64131